

# 3D Heteroatom-Doped Carbon Nanomaterials as Multifunctional Metal-Free Catalysts for Integrated Energy Devices

Rajib Paul, Feng Du, Liming Dai,\* Yong Ding, Zhong Lin Wang,\* Fei Wei, and Ajit Roy\*

Sustainable and cost-effective energy generation has become crucial for fulfilling present energy requirements. For this purpose, the development of cheap, scalable, efficient, and reliable catalysts is essential. Carbon-based heteroatom-doped, 3D, and mesoporous electrodes are very promising as catalysts for electrochemical energy conversion and storage. Various carbon allotropes doped with a variety of heteroatoms can be utilized for cost-effective mass production of electrode materials. 3D porous carbon electrodes provide multiple advantages, such as large surface area, maximized exposure to active sites, 3D conductive pathways for efficient electron transport, and porous channels to facilitate electrolyte diffusion. However, it is challenging to synthesize and functionalize isotropic 3D carbon structures. Here, various synthesis processes of 3D porous carbon materials are summarized to understand how their physical and chemical properties together with heteroatom doping dictate the electrochemical catalytic performance. Prospects of attractive 3D carbon structural materials for energy conversion and efficient integrated energy systems are also discussed.

## 1. Introduction


Carbon atom is unique in forming covalent bonds, both  $\sigma$  and  $\pi$ , with neighboring carbon atoms in various hybridization

Dr. R. Paul, Dr. F. Du, Prof. L. Dai  
Department of Macromolecular Science and Engineering  
Case Western Reserve University  
Cleveland, OH 44106, USA  
E-mail: liming.dai@case.edu

Dr. Y. Ding, Prof. Z. L. Wang  
School of Materials Science and Engineering  
Georgia Institute of Technology  
Atlanta, GA 30332-0245, USA  
E-mail: zhong.wang@mse.gatech.edu

Prof. F. Wei  
Department of Chemical Engineering  
Tsinghua University  
Beijing 100084, China

Dr. A. Roy  
Materials and Manufacturing Directorate  
Air Force Research Laboratory  
Wright-Patterson AFB  
Dayton, OH 45433, USA  
E-mail: ajit.roy@us.af.mil

 The ORCID identification number(s) for the author(s) of this article can be found under <https://doi.org/10.1002/adma.201805598>.

DOI: 10.1002/adma.201805598

states, such as  $sp$ ,  $sp^2$ ,  $sp^3$  or with other nonmetallic elements, generally called heteroatoms. This feature provides a variety of carbon allotropic structures, from single molecules to layered structures and to complex mesoporous architectures.<sup>[1–3]</sup> Carbon was first identified about 200 years ago within organic molecules and as building blocks for biomolecules. Later, natural carbon was discovered in the form of diamond, graphite, and amorphous carbon. Diamond is a very well-known hardest and transparent electrical insulator but a thermal conductor. It is a form of tetrahedral  $sp^3$  carbon atoms. Diamond has a unique crystal structure consisting of two interpenetrating face centered cubic Bravais lattices. On the contrary, graphite is soft and opaque having attractive electrical conductivity. It is basically a stack-up form of atomically thin (0.335 nm) graphene layers that are weakly bonded by van der

Waals forces. The graphene monolayers are hexagonal packed lattice of  $sp^2$ -hybridized carbon atoms.<sup>[4,5]</sup> Clearly, the diversity in atomic arrangements can provide various allotropic structures of carbon, which are different in physical and functional properties.<sup>[6–11]</sup> Motivated by this fact, there have been seminal quests for inventing new nanostructured carbon allotropes with various dimensions, such as 0D, 1D, 2D, and 3D.

The recent discoveries of carbon nanomaterials added new members to the carbon family. In 1985, fullerene ( $C_{60}$ ) was the first discovered as carbon nanostructure with 0 dimension.<sup>[12,13]</sup> About 6 years later, another 1D carbon allotrope was discovered, called carbon nanotubes (CNTs), whose structure was proposed by Iijima.<sup>[14,15]</sup> In general, CNTs (both single- and multiwalled CNTs, abbreviated as SWNTs and MWNTs) are utilized as reinforcements in composite materials having different polymer matrices and as building blocks for numerous catalysts and electrodes.<sup>[16,17]</sup> In 2004, the most widely investigated and used 2D carbon nanostructure, called graphene, was experimentally evidenced and characterized by Geim and Novoselov, although it was predicted and identified decades ago.<sup>[1]</sup> The graphene family type is ever increasing since its discovery. Different manufacturing processes yield graphene products diverse in size, thickness, and impurities. Thereafter, research interests on graphene quantum dots (GQDs) or carbon dots (C-dots) have been reported till now. Structurally, GQD or C-dot is graphene of mono- or few-layers with distinct but interesting

optoelectronic properties.<sup>[18,19]</sup> Although these low-dimensional carbon nanostructures (0D, 1D, and 2D) have been adapted for many functional applications due to their excellent intrinsic physicochemical properties, they are often suffered from inferior extrinsic characteristics, such as poor electrical and thermal conductivities, low effective surface areas, and unreliable mechanical properties.<sup>[20–25]</sup>

To address this problem, hierarchical carbon materials having porous structure in three dimensions are being pursued. Such 3D mesoporous carbon material construct possibly would provide a desirable backbone support of enhanced surface area for catalytically active sites, a multidimensional conductive network for improved electron transport, and an expanded volume to accommodate the electrolyte/reactant diffusion with significantly improved mechanical stability. To date, most of the reported 3D carbon materials are basically agglomerated or simply assembled from lower dimensional carbon nanostructures, which are widely used for electrocatalytic applications,<sup>[16,26–28]</sup> though there have been a few successful reports on fabricating isotropic 3D porous electrodes.<sup>[29]</sup> Heteroatom doping in carbon nanostructures is also crucial for increasing the efficiency to realize multifunctional electrocatalysts.<sup>[30]</sup> In fact, multifunctional 3D nanomaterials are promising to fabricate various integrated devices for fulfilling the soaring energy requirements, as well as infuse technological advancement toward efficient, reliable, multifunctional, portable, and flexible devices.<sup>[16,31]</sup> Here, we provide a comprehensive and critical overview on mesoporous 3D heteroatom-doped carbon nanomaterials as multifunctional metal-free catalysts for integrated energy devices by summarizing and discussing advancement in fabrication methods of undoped and heteroatom-doped (multiatom doped) 3D carbon catalysts from lower dimensional carbon nanostructures. Also, we discuss isotropic 3D carbon structure fabrication for efficient multifunctional energy conversion and storage applications, along with illustration of various factors influencing their performance and applicability.

## 2. Different Allotropes of Carbon

Allotropes are different structural forms of an element. Various allotropic forms of carbon with different dimensions, such as 0D (e.g., fullerene, onion-like carbon, C-dot, GQD, nanodiamond), 1D (e.g., SWNT and MWNT, nanohorns, partially and fully unzipped nanotubes), 2D (e.g., monolayer and multilayer graphene, amorphous, graphitic, and diamond-like carbon films), and 3D (e.g., graphite, diamond, and pillared graphene) carbons, are depicted in **Figure 1a**.<sup>[1,32]</sup> At present carbon-based 3D mesoporous metal-free catalysts have become very interesting for different electrochemical-reaction-based energy storage applications.<sup>[33–35]</sup> Such mesoporous 3D carbon can also be fabricated using any of the above-mentioned individual or combined allotropes. However, pillared graphene is an ideal and isotropic 3D mesoporous structure predicted to possess superior charge transport properties to other 3D carbon structures obtained through simple physical or chemical combination or agglomeration.

Graphene oxide (GO) is the latest, but the most popular graphene flake, which is cheap, soluble in different solvents, and



**Rajib Paul** studied with a bachelor and a master degree in physics, and a Ph.D. degree in materials science and nanotechnology from Jadavpur University, Kolkata, and joined as a postdoctoral researcher at Birk Nanotechnology Center in Purdue University before moving to Case Western Reserve University. He has extensive expertise in synthesis and nanostructuring of mesoporous carbon materials using various plasma induced

and thermal CVD for efficient energy storage and conversion, mechanically stable hard coatings, and optoelectronics applications. His research interest is also extended to characterizing thermomechanical properties in 3D hierarchical carbon materials and structural battery fabrication for unmanned electric air vehicles.



**Liming Dai** is a Kent Hale Smith Professor in the Department of Macromolecular Science and Engineering at Case Western Reserve University and is also the director of the Center of Advanced Science and Engineering for Carbon (Case4Carbon). He received a B.Sc. degree from Zhejiang University in 1983, and a Ph.D. degree from the Australian National University in 1991. Before joining the CWRU, he was with CSIR, Australia,

the University of Akron and the University of Dayton as the WBI Endowed Chair Professor. His expertise lies across several fields, including the synthesis and functionalization of polymers and carbon nanomaterials for energy and biorelated devices.



**Ajit Roy** is Principal Materials Research Engineer at the Materials and Manufacturing Directorate, Air Force Research Laboratory (AFRL). His research expertise includes functional materials, materials modeling and processing, 3D nanostructure, 3D composites, carbon foam, and carbon-carbon composites. Prior to AFRL, he was affiliated with the University of Dayton Research Institute (UDRI) for 10 years.

His current research activities include multifunctional materials, laser-material interactions, strain-resilient electronics, energy transport in nanomaterials, behavior and failure mechanisms in nanomaterials and hybrid graphitic (carbon) foam, and nanomechanics.

primary choice for fabricating 3D hybrid carbon electrodes via chemical routes.<sup>[2,16,23,36,40]</sup> GO is generally prepared from graphite flakes through intense oxidation using  $\text{KMnO}_4$  and

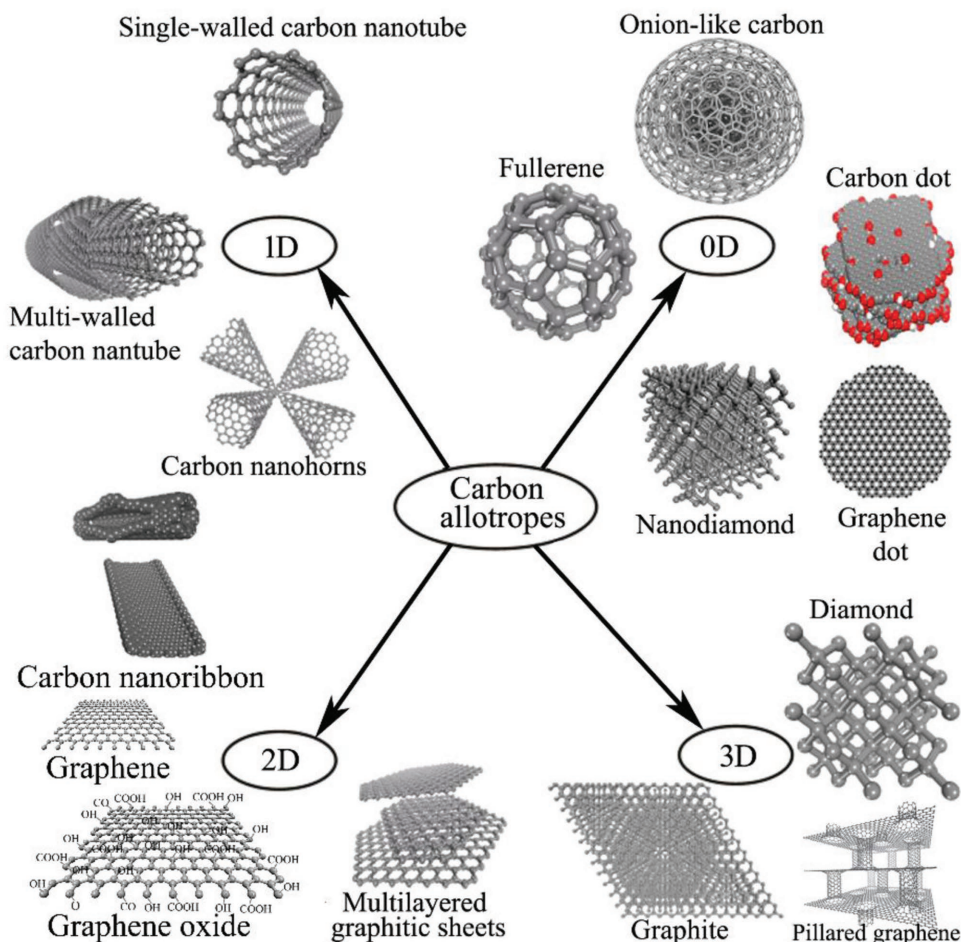


**Figure 1.** Carbon allotropes in different dimensions. All images except for graphene, graphene oxide, and pillared graphene: Adapted with permission.<sup>[1]</sup> Copyright 2015, American Chemical Society. Images for graphene, graphene oxide, and pillared graphene: Reproduced with permission.<sup>[32]</sup> Copyright 2015, AIP Publishing.

concentrated  $\text{H}_2\text{SO}_4$  and  $\text{H}_3\text{PO}_4$  in a controlled chemical process followed by elongated  $\text{H}_2\text{O}_2$  treatment near  $0^\circ\text{C}$ , filtration, cleaning, and drying processes.<sup>[36,37]</sup> The functional properties of 3D carbon nanostructures depend on the constituting carbon allotrope(s) and their physicochemical states, the fabrication process, and the defect density and type of doped heteroatom(s), along with the electronic states of those dopants.<sup>[38,39]</sup>

### 3. Metal-Free Heteroatom-Doped Carbon

Precious-metal catalysts, particularly noble metals such as iridium, palladium, and platinum and associated alloys, have remained the most attractive electrode materials for different electrocatalytic chemical reactions for energy storage and conversion.<sup>[41]</sup> However, their low selectivity, limited availability, high cost, poor durability, affinity toward gas poisoning, and related potential adverse impact to environment have so far hindered their industrial scale acceptance.<sup>[42]</sup> Henceforth, serious efforts are now pursued to replace them with cost-effective and environmentally friendly alternatives. In this context, nonprecious transition metals (Ti, W, Sn, Zn, Fe, Co,

Mo, and Ni), their carbide, nitride, oxide, carbonitride, and oxynitride catalysts have been and still being widely investigated.<sup>[41–48]</sup> However, the low intrinsic conductivities of such nonprecious-metal-based catalysts, due to the interfacial complexity and thermodynamic instability of its hybrid structures, limit its application domain. Recently, carbon-based catalysts have emerged as promising alternatives and are increasingly being utilized as efficient catalysts due to their low density, high specific surface area, suitable electrical and thermal conductivities, chemical stability, and suitable mechanical properties.<sup>[2,3,23,40,48]</sup>

Carbon-based heteroatom-doped nanomaterials were first introduced in 2009 which, as metal-free catalysts, are comparable to platinum for efficiently catalyzing oxygen reduction reaction (ORR) in fuel cells.<sup>[49,50]</sup> Thereafter, this new class of carbon-based electrocatalysts has been reported to also be efficient in oxygen evolution reaction (OER), hydrogen evolution reaction (HER), and many catalytic reactions,<sup>[2,51–54]</sup> including catalysis of  $\text{I}^-/\text{I}_3^-$  for dye-sensitized solar cells<sup>[2]</sup> and  $\text{CO}_2$  reduction reaction ( $\text{CO}_2\text{RR}$ ) for numerous applications, namely, biosensing, hydrocarbon-based fuel production,<sup>[44]</sup> monitoring environmental effects,<sup>[52]</sup> and even for commodity chemicals

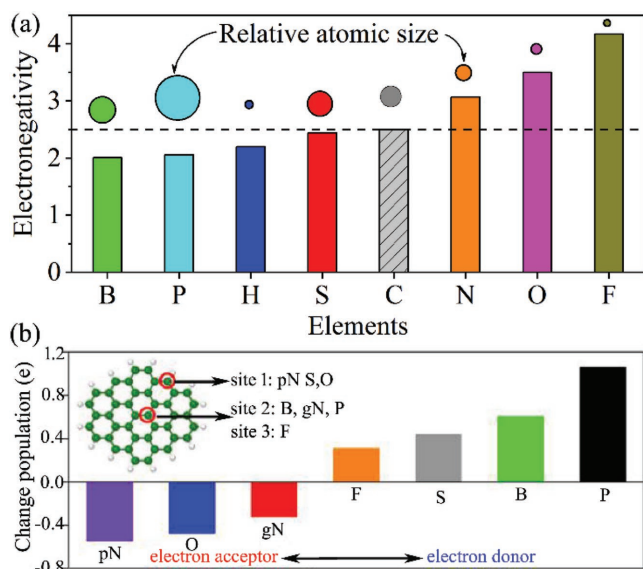


**Figure 2.** a) Comparison of electronegativity for popular heteroatoms doped in carbon nanomaterials for electrochemical energy storage with their relative atomic size. b) Analysis of natural bond orbital population for six nonmetallic heteroatoms doped in graphene lattice (pN: pyridinic; gN: graphitic N). Inset: The predicted doping location for various elements. Site 1: edge; site 2: in-plane center; site 3: out-of-plane center on graphene. b) Reproduced with permission.<sup>[74]</sup> Copyright 2014, American Chemical Society.

production.<sup>[2,53,54]</sup> More recently, multidoped heteroatom carbon nanostructured electrode materials have demonstrated excellent metal-free multifunctional electrocatalysis for ORR, OER, and HER utilized in rechargeable Zn–air (primarily metal–air) batteries,<sup>[48]</sup> regenerative fuel cells,<sup>[55]</sup> and simultaneous ORR, OER, and HER reactions.<sup>[39,56,57]</sup> Such carbon-based heteroatom-doped single or multifunctional metal-free electrocatalysts' performance is often superior to that of noble metal and transition metal catalysts. Notable phenomena of charge induction/modulation around the heteroatom-doped carbon lattice and transport property modulation often contribute to such attractive performance enhancement<sup>[2,49]</sup>

In fact, the C–C bond is nonpolar, but carbon atoms can form polar bonds with heteroatoms to impose different dipole moments depending on their difference in electronegativity (e.g., electronegativity,  $\epsilon = 2.50$  for C,  $\epsilon = 3.07$  for N) and atomic size from those of the carbon atom (Figure 2a). Therefore, a change in the density of states and charge population is attained on both the carbon atom and heteroatom to impart catalytic activities to various heteroatom-doped graphitic carbon materials.<sup>[58–68]</sup> The properties of nitrogen-doped  $sp^2$  carbon nanomaterials are also altered by the chemical state of nitrogen atom doped onto the carbon lattice. It can be pyridinic, pyrrolic, graphitic, or oxidized N state.<sup>[69]</sup> Although, it is controversial to comment on their differentiation based on the electrocatalytic activity.<sup>[70]</sup> However, quantum mechanical calculations and experimental investigations indicate that pyridinic N and graphitic N can be beneficial for electrocatalysis in ORR by facilitating  $O_2$  adsorption onto the neighboring carbon atoms. This facilitates the four-electron pathway for ORR.<sup>[69,71–73]</sup> Additionally, sulfur (S;  $\epsilon = 2.44$ ) doped carbon catalysts are

studied for ORR applications.<sup>[30,48]</sup> Codoping and tridoping with various heteroatoms, among N, boron (B,  $\epsilon = 2.01$ ), S, phosphorus (P,  $\epsilon = 2.06$ ), fluorine (F,  $\epsilon = 4.17$ ), and oxygen (O,  $\epsilon = 3.50$ ), have recently been introduced for fabricating multifunctional metal-free catalysts for electrochemical energy conversion and storage.<sup>[55,57]</sup>

The natural bond orbital (NBO) population analyzed by density functional theory (DFT) shows that different heteroatoms acquire different amount of charge populations within graphene lattice. For example, N and O being negatively charged relative to the adjacent C atom culminate as electron acceptors, whereas F, S, B, and P act as donors because they accumulate positive charge.<sup>[74]</sup> Figure 2b shows the NBO population and the free energy diagrams for HER. In fact, the codoping, tridoping, and even more than three heteroatoms doping in carbon lattice have often been observed to perform synergistic effects toward electrochemical activities. The electrocatalytic performance of 3D carbon-based electrodes depends on the synthesis and fabrication process, type and amount of heteroatom doping, active surface area, extrinsic conducting properties, interfacial resistive and chemical properties at the junctions, length of diffusion pathways, as well as the nature and size of pores and preadsorbed entities therein.<sup>[2,3,17,23,30]</sup> Table 1 compares the experimentally obtained physical properties of various carbon materials with different dimensions.<sup>[3,16,75–91]</sup>

#### 4. Synthesis of 3D Carbon Materials and Heteroatom Doping

Various chemical vapor deposition (CVD), physical vapor deposition (PVD), chemical processing, pyrolysis, 3D printing, and various assembly-based techniques have been devised to fabricate 3D carbon materials (Table 1) for electrochemical energy storage and conversion applications.<sup>[92–95]</sup> Owing to the high efficiency and mechanical stability for electrochemical energy storage, CNT–graphene-based 3D carbon materials, prepared normally by solution processed assembly,<sup>[96–102]</sup> layer-by-layer assembly,<sup>[103–107]</sup> and vacuum filtration,<sup>[108–110]</sup> have been widely studied. The product of assembly processes is generally of inferior quality that would ultimately affect the conductivity and surface area, though this method is simpler than in situ CVD. In situ growth of graphene–CNT hybrid 3D structures (e.g., pillared graphene in Figure 1) is more complicated, but holds better control of the product quality, including their morphology, density, and desired orientation of the hybrid structures. Therefore, different in situ techniques, such as CVD,<sup>[111–125]</sup> templated CVD,<sup>[17,29,126,127]</sup> and chemical unzipping,<sup>[16,128,129]</sup> have recently become very popular. Figure 3 shows CVD methods, with and without a template, for the synthesis of 3D carbon structures.<sup>[17,29,125,126,128]</sup> As compared to other CVD techniques, in the templated CVD method particular structural designing is easily achieved. However, comparatively this technique often comes out to be a multistep process, complex and expensive. Mass production of porous 3D carbon electrodes can easily be produced through chemical processes although they are inferior in terms of selectively introducing chemical contents, conducting properties and mechanical integrity. Therefore, a high-temperature postpyrolysis step is

**Table 1.** Properties of different carbon allotropes.

Material (dimension)	Synthesis method	BET surface area <sup>a)</sup> [m <sup>2</sup> g <sup>-1</sup> ]	Thermal conductivity [W <sup>-1</sup> m <sup>-1</sup> k <sup>-1</sup> ]	Electrical conductivity [S cm <sup>-1</sup> ]	Ref.
Fullerene (0D)	Arc discharge	80–90	0.4	10 <sup>-10</sup>	[75]
Fullerene shoot (0D)	Arc discharge of carbon rod	175	–	–	[76]
Fullerene shoot–CO <sub>2</sub> or Ar pyrolyzed (0D)	Arc discharge + gas pyrolysis	345–346	–	–	[76]
Fullerene shoot–KOH activated (0D)	Depleted and KOH activated	2153	–	–	[77]
Nanodiamond (0D)	Microwave plasma CVD	≈400–600	1–12	100–10 <sup>-10</sup>	[78–80]
SWCNT (1D)	CVD	≈1300	2000–6000	–	[75,78,81]
MWCNT (1D)	CVD + purify	≈450	3000–3500	–	[78,81,82]
MWCNT–KOH activated (1D)	CVD + chemical activation	≈785	–	–	[16]
Graphene or G (2D)	CVD	≈1500	5000	≈2000 to 10 <sup>6</sup>	[3,75]
Graphene oxide (2D)	Chemical reduction of graphite	≈423–3100	–	–	[16,83]
Graphite (3D)	Natural or synthetic	≈10–20	≈1500–2000 and 5–10 (cross-plane)	2–3 × 10 <sup>4</sup> and 6 (cross-plane)	[75]
Diamond (3D)	Natural or synthetic	20–160	900–2320	10 <sup>-11</sup> to 10 <sup>-18</sup> (insulator)	[84,85]
GO+CNT (3D)	Agglomeration and chemical reduction	≈435	–	–	[83]
Mesoporous C from rGO (3D)	Microwave irradiation+ KOH activation	≈3290	–	–	[16]
N-doped macro/mesoporous C (3D)	Macro/mesoporous silica as a hard template associated with furfuryl alcohol	≈1826	–	–	[87]
Hydrogel with B- and N-codoped porous C networks (3D)	Agarose hydrogel pyrolysis containing TBE buffer with KOH activation	≈2666	–	–	[88]
N/P/O–graphene (3G)	Mixture of artemia cyst shells and red P ball milled: KOH activation/pyrolysis at 850 °C	≈1406	–	–	[89]
N–C microtube sponge (flexible) (3D)	Facial cotton pyrolysis at 1000 °C under NH <sub>3</sub> for 1 h	≈2358	–	–	[90]
P/S C <sub>3</sub> N <sub>4</sub> sponge sandwiched with C nanocrystals (3D)	Pyrolysis at 500 °C followed by freeze-drying	≈1474	–	–	[91]

<sup>a)</sup>Detailed atomic representation in Brunauer–Emmett–Teller (BET) surface area is available in cited respective references.

normally applied to reduce chemical impurity and increase conductive properties.<sup>[16,23]</sup> Besides, carbon aerogels, xerogels, and hydrogels have also been fabricated via chemical routes as low density efficient electrodes.<sup>[16]</sup> In this context, it would be important to mention that a template-assisted chemical process followed by postpyrolysis step may be interesting to provide particular hierarchy in 3D carbon electrodes.

Recently, 3D carbon electrodes, including MOF-derived mesoporous carbon structures and carbide-derived carbon and onion-like carbon structures,<sup>[73,130]</sup> have been prepared by solution-based chemical processes, condensation, and coordination reactions. Other major printing techniques, such as inkjet printing, screen printing, and transfer printing, have also been commonly used for depositing nanostructured carbons onto substrates of varying size, surface energy, and flexibility for energy applications, though 3D printing is an emerging technology.<sup>[131–141]</sup> 3D printing can offer porous carbon structures of 10 μm thick or thicker with very quick drying time (few seconds).<sup>[130–134]</sup> Carbon allotropic nanomaterials combined with various polymers have been used as highly viscous inks for fabricating 3D-printed carbon structures for Li-ion batteries, supercapacitors, water splitting electrolyzers, fuel cells, and environmental protection applications.<sup>[133–137]</sup> **Figure 4** illustrates various electrodes fabricated by different 3D printing methods.

Heteroatom doping into (3D) carbon nanomaterials can be performed in two ways: during synthesis and postsynthesis. For in situ heteroatom doping during the synthesis of carbon materials, various heteroatom-containing chemical reagents are mixed with carbon sources as precursors or by synthesizing in different heteroatom-containing gas environments. Postsynthesis heteroatom doping can be obtained through numerous chemical reactions, and pyrolysis of precursors in the presence of various chemical reagents and gases or by plasma treatments. The carbon structures thus obtained are often processed through activation steps, either by heating with KOH or H<sub>2</sub>SO<sub>4</sub> solution (at a low-temperature (≈100–200 °C) chemical activation) or pyrolysis at a high temperature (≈700–1000 °C) with gases, such as HN<sub>3</sub>, N<sub>2</sub>, H<sub>2</sub>, and CO<sub>2</sub> (called gas activation).<sup>[3,16]</sup> Sometimes some low carbon-containing precursors are carbonized or graphitized to maximize its carbon constituents or crystallinity and then it is activated in inert or gaseous environments. This whole process is called physical activation of carbon materials. Heteroatom-doped carbon nanostructures are generally obtained through this method from various polymers or petroleum products.<sup>[2,3,16]</sup> 3D printing of isotropic heteroatom-doped carbon nanostructures can also be very interesting to conceive.

The chemical activation temperature is generally lower than in physical activation process. Therefore, the probability of

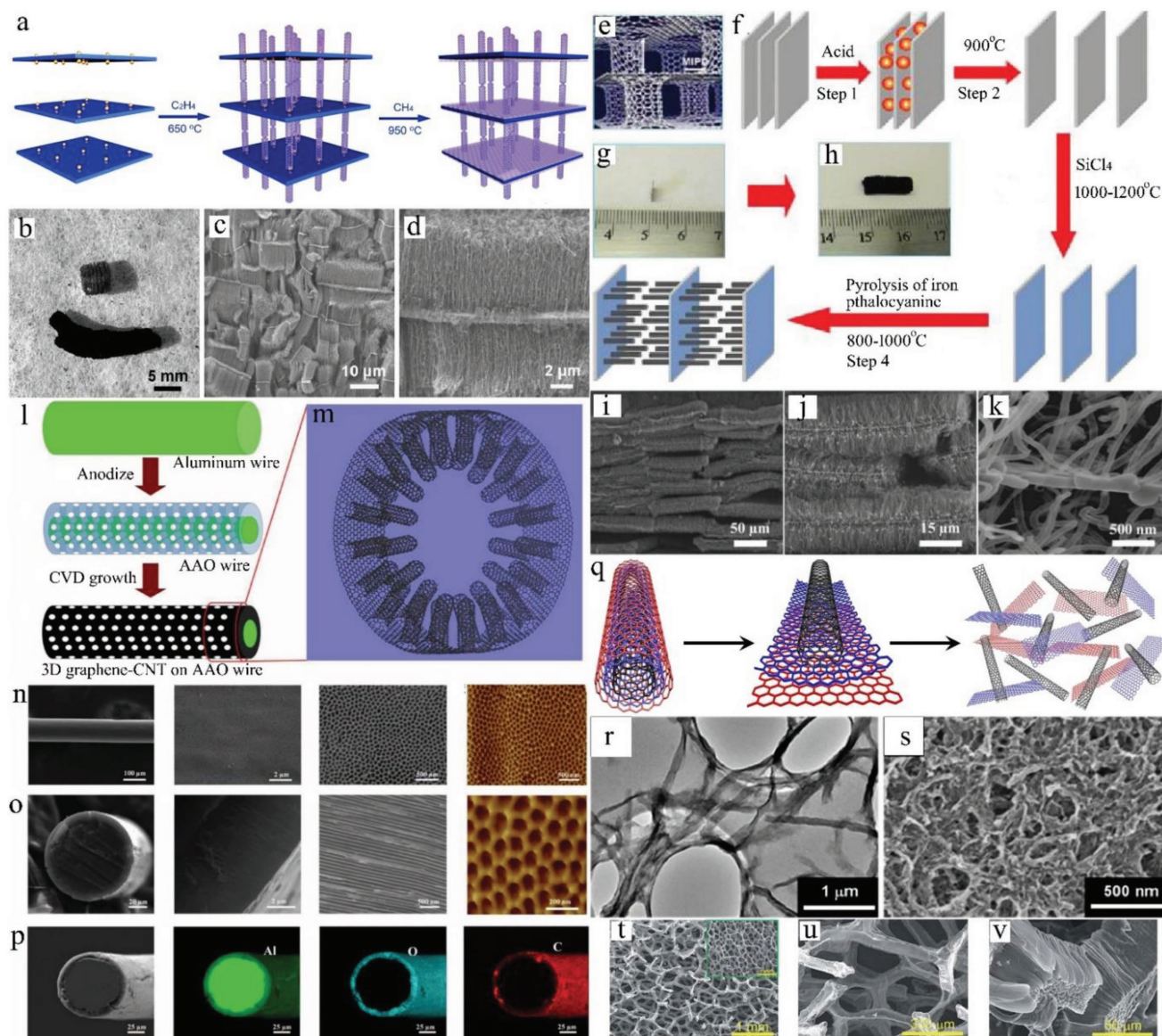


**Figure 3.** a) Schematic for synthesis of aligned CNT/graphene sandwiches on bifunctional catalysts graphene sandwiches, b) digital photograph of a block of EV catalyst (brown) and aligned CNT/graphene sandwich and c, d) SEM of aligned CNT/graphene/EV composite. a–d) Reproduced with permission.<sup>[125]</sup> Copyright 2014, Elsevier Inc. e) Schematic of 3D pillared VACNT–graphene architecture. f) Detailed procedure for fabrication of 3D pillared VACNT–graphene structure. g, h) Digital images of HOPG with 80  $\mu\text{m}$  thickness (g) and thermally expanded VACNT intercalated graphene layers (h). i–k) SEM of 3D pillared VACNT–graphene nanostructures. e–k) Reproduced with permission.<sup>[126]</sup> Copyright 2013, American Chemical Society. l, m) Schematic of synthesis procedure and structural details of 3D graphene–RACNT fiber. n, o) SEM and AFM images of the 3D graphene–RACNT fiber, and p) its SEM and EDX elemental mapping. l–p) Reproduced with permission.<sup>[29]</sup> Copyright 2015, American Association for the Advancement of Science. q) Schematic formation of the GONR/CNT hybrid, and r, s) its TEM and SEM images. q–s) Reproduced with permission.<sup>[128]</sup> Copyright 2013, Wiley-VCH. t–v) SEM of 3D CNT foam obtained by growing VACNTs on Ni foam template by MPCVD, inset of (t) shows bare Ni foam. t–v) Reproduced with permission.<sup>[17]</sup> Copyright 2016, Royal Society of Chemistry.

the formation of porous architectures is higher in the chemical activation process although proper gas bubbling strategy during the physical activation process can produce microporous or sometimes mesoporous materials with high graphitic crystallinity.<sup>[3,11]</sup> Frankly speaking, the chemical activation process needs a product postcleaning step to reduce the residual chemicals from the final carbon product.<sup>[11,36,37]</sup> The specific surface area of the heteroatom-doped carbon structures and their catalytic properties are also dependent on the activation process parameters used. However, more research is required

to confidently comment on such controversial issues. N-doped carbon nanostructured materials have been widely used for electrochemical catalytic applications.<sup>[2,3]</sup> Besides N and other single heteroatom doping, such as O, B, S, P, and different halogens (i.e., F, Cl, Br, and I), the codoping of NS, BN, NP, NF, PS, and tridoping (such as NPO, etc.) into carbon materials has been performed as discussed in detail in the following sections. The density function theory indicates that the heteroatom doping into carbon lattice modulates the charge distribution characteristics to the adjacent C atom and this modifies the

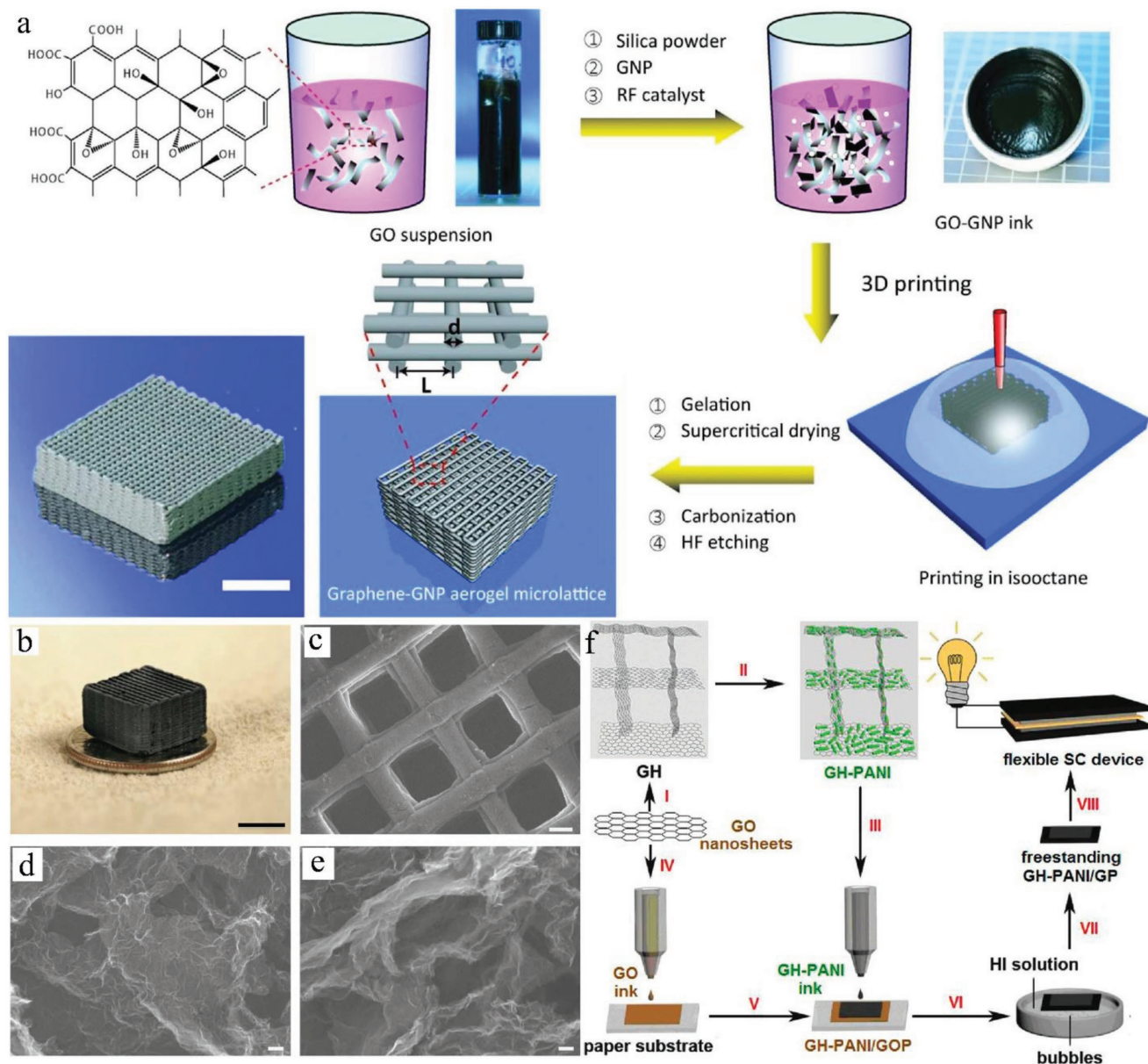


**Figure 4.** a) Schematic of fabrication steps for 3D-printed graphene composite aerogels (3D-GCA). Reproduced with permission.<sup>[135]</sup> Copyright 2016, American Chemical Society. b) Digital image and c–e) SEM images of 3D-printed microlattice using graphene aerogel (c), and graphene aerogel without (d) and with 4 wt% R–F (e) after etching. b–e) Reproduced with permission.<sup>[136]</sup> Copyright 2015, Macmillan Publishers Limited. f) Step I: self-assembled 3D graphene hydrogel (GH) from GO sheets; Step II: in situ polymerization of PANI onto GH; Step III: ball milling and ultrasonic exposure of 3D GH–PANI composite for GH–PANI ink preparation; Step IV: GOP formation by printing GO ink on paper; Step V: overprinting of GH–PANI inks onto GOP; Step VI: soaking of GH–PANI/GOP in diluted HI; Step VII: simultaneous reduction of GH–PANI/GOP using HI and formation of freestanding GH–PANI/GP after peeling off; Step VIII: fabrication of flexible supercapacitor (SC) device using gel electrolyte onto GH–PANI/GP electrode. Reproduced with permission.<sup>[137]</sup> Copyright 2014, American Chemical Society.

related electrocatalytic performance. Therefore, different heteroatom/heteroatom incorporation relates to modification in electrochemical performance in different degrees for different catalytic reactions (such as ORR, OER, and HER). Codoping and tridoping have been established by numerous studies to be beneficial for such electrocatalytic applications which are often overlooked as synergistic effects. Therefore, more detailed study is required to clearly understand the mechanism of multidoping effect on electrochemical catalysis.

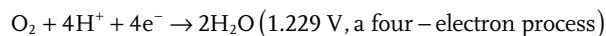
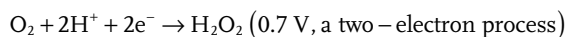
## 5. Mesoporous 3D Carbon as Catalysts for Oxygen Reduction Reaction

For the biological respiration process, ORR is a crucial reaction and it is also technologically important in energy-converting systems, such as metal–air batteries and fuel cells, etc.<sup>[3,30,67]</sup> There are different types of fuel cells. As compared to other fuel cells, solid-oxide-based high-temperature fuel cells (SOFCs), polymer-electrolyte-based membrane fuel cells (such

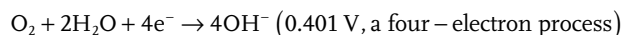
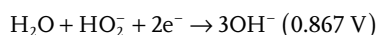
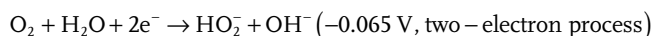
as proton-exchange-membrane fuel cells, PEMFCs), and direct alcohol-based fuel cells (for example, direct methanol fuel cell, DMFC) are very well known for having lower temperature of operation and longer cell life. These fuel cells are very promising for futuristic lightweight electric vehicles as well as portable electronics.<sup>[142]</sup> In both PEMFC and DMFC, precious Pt-based catalyst, the key component, is mounted together with a mesoporous conducting material (such as carbon black) either as anode or cathode, for electrocatalysis of hydrogen (named as hydrogen oxidation reaction, HOR) and alcohol (termed as alcohol oxidation reaction, AOR) or oxygen (called oxygen reduction reaction), distinctively. However, the lethargic reaction kinetics for HOR and AOR at relatively low operating temperature of 80–100 °C as well as high energy input necessary for ORR induces a large polarization resistance.

ORR occurs in multisteps related either to a four-electron ( $4e^-$ ) path for direct  $H_2O$  generation in acidic electrolyte and  $OH^-$  production in alkaline electrolyte or a two-electron ( $2e^-$ ) process forming  $H_2O_2$  in acidic electrolyte and  $HO_2^-$  emission in alkaline electrolyte as intermediate products. Such reaction pathway mainly depends on the inherent electrochemical catalytic characteristics of the electrodes. The usual reaction mechanisms in the presence of different electrodes and media of varied thermodynamic potential, operating under standard condition, is presented below:<sup>[143,144]</sup>

ORR in acidic electrolyte



ORR in alkaline electrolyte



For a given electrocatalyst, a selection of higher  $4e^-$  reduction pathway facilitates a superior ORR electrocatalysis.

Nanoparticulated Pt catalyst is considered as the best electrocatalyst for the ORR since long past, although with concerns of high related cost and scarcity which have prejudiced the fuel cells from industrialization. With an aim to reduce or even completely replace Pt-based catalysts with alternatives with lower cost, there have been tremendous research studies. We had previously discovered that heteroatom-doped graphitic carbon nanomaterials (for example, CNTs, graphene) could act as metal-free ORR catalysts with reduced cost and comparable efficiency in fuel cells.<sup>[2,3,49,145]</sup> Among heteroatom-doped 3D carbon catalysts, nitrogen doping in varied carbon architectures, including MWCNT–rGO hybrids, rGO-based aerogels, xerogels, hydrogels, porous carbon (meso- and macroporous), graphene foams, carbon capsules, polymer, and MOF-derived carbon networks, has been reported in the literature.<sup>[58–64,66,67,84,87,146–171]</sup> Carbon nitride ( $C_3N_4$ )-based carbon composites,<sup>[67,73,169–171]</sup>

graphene foams,<sup>[172–174]</sup> and S-doped carbon aerogel have also been extensively studied for ORR applications. Furthermore, S/N,<sup>[175–185]</sup> B/N,<sup>[88,186–188]</sup> P/N<sup>[189–192]</sup> and F/N<sup>[193,194]</sup> codoping and N/P/O<sup>[119]</sup> tridoping have recently been achieved to demonstrate the bifunctional and trifunctional carbon-based electrocatalysis for energy storage and conversion.

Nitrogen-doped porous 3D carbon materials are very well known for their high ORR activity and exceptional conductivity, along with good retentivity. For instance, N-doped mesoporous graphitic stacks (arrays) showed high electrocatalytic activity, stability, and methanol tolerance in alkaline solutions.<sup>[60]</sup> Furthermore, an aerogel based on N-doped graphene nanoribbons (GNRs) acted superb ORR electrocatalytic performance and superior stability compared to commercial Pt/C in alkaline as well as acidic media.<sup>[61]</sup> In another effort, N-doped carbon nanofiber (N-CNF) exhibited high N content (5.8 at%), high active-site density related to N-doping, and high BET surface area about  $916 \text{ m}^2 \text{ g}^{-1}$ .<sup>[157]</sup> This N-CNF-based aerogel has also exhibited excellent ORR activity with 0.85 V onset potential versus reversible hydrogen electrode (RHE), high (3.97 at 0.8 V) electron-transfer number, and attractive electrochemical ORR stability of about 97.5% retention even at 10 000 potential cycles (0.1 M KOH).<sup>[157]</sup> This N-CNF aerogel has also demonstrated a 0.83 V onset potential in 0.5 M  $H_2SO_4$  media,<sup>[157]</sup> which is very promising performance worth mentioning.

Hierarchically N-doped cross-linked porous 3D carbons called LHNHPC structure possess a specific surface area of  $2600 \text{ m}^2 \text{ g}^{-1}$ , 3.12 at% N-dopants, and an ORR activity closely comparable to Pt/C catalyst, the benchmark in basic media.<sup>[84]</sup> Such excellent electrochemical properties have often been attributed to the synergistic effects arising due to the mesoporous structure, doped N-heteroatoms, and the high specific surface area.<sup>[84]</sup>

**Table 2** summarizes important reports on various N-doped and S-doped 3D carbon materials for ORR application. Among them, it is worth to note that S-doped 3D aerogel and graphene foam showed superior ORR performance to their undoped carbon structures (Table 2),<sup>[172,173]</sup> although sulfur has identical electronegativity as of carbon implying that the doping-induced charge-transfer remains neutral. However, the hydrophobic nature of the thiophene-like form of S within the carbon lattice plays a crucial role in drawing oxygen out of the electrolyte that facilitates its physical adsorption on the electrode surface, primarily enhances the ORR mechanics.<sup>[73,173]</sup> Other bulky oxygen-containing sulfur surface groups (e.g., sulfonic acids, sulfoxide, sulfones) situated in larger pores have also been demonstrated to attract electrolyte solutions containing dissolved oxygen toward the pore system.<sup>[174]</sup> However, possible contributions to the enhanced ORR performance by the sulfur-doping induced spin redistribution cannot be ruled out.<sup>[175]</sup> Therefore, further more research is needed to explore the S-doping effect on ORR activities in 3D hierarchically porous carbon materials.

N- and S-codoped hollow 3D carbon-sphere (porous) nanocomposites (N,S-hcs) demonstrated excellent ORR electrocatalytic performance (**Figure 5a–e**) with a four-electron transfer pathway, appreciable durability, and high tolerance to methanol crossover/CO-poisoning effects.<sup>[180]</sup> This work demonstrates the synergistic effect associated with heteroatom codoping into porous C structures.<sup>[181]</sup>



**Table 2.** Nitrogen- or sulfur-doped 3D porous carbon catalysts for ORR.

Material	Synthesis method	Chemical content and property	Electrolyte	Onset potential [V vs RHE] and <i>n</i>	Tafel slope [mV per decade]	Stability	Ref.
MWCNT-rGO hybrid	Poly(diallyldimethylammonium chloride functionalized hydrophilic MWNTs and rGO electrostatic self-assembly)	rGO/pMWNT ≈ 1:2; the charge/g: 2.66 C/g for rGO, 2.16 C/g for pMWNTs and 62.9 C/g for rGO/pMWNT (0.5:1)	0.1 M KOH	0.8 V, 3.6–3.3		61% after 20 000 s	[146]
rGO/activated carbon aerogel	GO+ activated carbon+ ammonium hydroxide, autoclaved (12 h), lyophilized (12 h)	SA = 758.19 m <sup>2</sup> g <sup>-1</sup>	0.1 M KOH	0.83 V, 3.52		–	[147]
N-G flower	Co-pyrolysis (500–700 °C) of melamine and ferrocene	N-3.62 at%, SA ≈ 670 m <sup>2</sup> g <sup>-1</sup>	0.1 M NaOH	0.87 V, 3.96		98.3 and 95.3% after 5000 cycles	[148]
N-graphene foam	Pyrolysis-900 °C of silica spheres, FeCl <sub>2</sub> ·4H <sub>2</sub> O, dicyandiamide and GO.	N-5.07%, SA ≈ 670 m <sup>2</sup> g <sup>-1</sup>	0.1 M KOH 0.1 M HClO <sub>4</sub>	0.95 V (Pt/C-0.96), 3.9 0.83 V, 4		18% after 21 600 s	[149]
Hierarchical NG/porous C composite	GO/ethylenediamine, 950 °C	SA ≈ 1510.83 m <sup>2</sup> g <sup>-1</sup>	0.1 M KOH	0.91 V, 3.79	70 mV per decade (68 for Pt/C)		[58]
3D NG	Pyrolysis of GO+polypyrrole, 900 °C	2–3%, SA ≈ 370 m <sup>2</sup> g <sup>-1</sup>	0.1 M KOH	0.83 V, 3.9		min. after 2000 cycles	[59]
N-G nanoribbon aerogel	Chemical unzipping of MWNTs, hydrothermal mixing with pyrrole, pyrolysis	SA = 480–617 m <sup>2</sup> g <sup>-1</sup> , density ≈ 2.5–22 mg cm <sup>-3</sup>	0.1 M KOH	0.81 V, 3.66–3.92		78% after 20 000 s	[61]
N-C xerogel	Pyrolysis of organic xerogel in NH <sub>3</sub> and pyrolyate	SA = 541 m <sup>2</sup> g <sup>-1</sup>	0.5 M H <sub>2</sub> SO <sub>4</sub>	0.84 V, 3.5–3.7	103 mV per decade (pt/C-72)		[62]
N-C aerogel	Pyrolysis-900 °C, organic aerogel (synthesized from glucose and borax)	N: 2.0–5.5 wt%, SA: ≈265 m <sup>2</sup> g <sup>-1</sup>	0.1 M KOH	≈0.81 V, 3.3		85%–200 min	[150]
3D Nanoporous N-G	CVD G growth on nanoporous Ni foam with pyridine—1000 °C	5%	0.1 M KOH	0.86 V, 3.9			[63]
3D flower-like N-C	Ferrocene and melamine: coprolysis at 500–700 °C	4.62%	0.1 M NaOH	0.87 V, 3.96			[148]
N-macro/meso-C	Hard templated macro/mesoporous silica in furfuryl alcohol	SA ≈ 1826 m <sup>2</sup> g <sup>-1</sup>	0.1 M KOH	0.87 V, 3.2	69.6 mV per decade	93.8% after the 45 000 s	[87]
N/CNTs nanotubes/ carbon nanofibers composite (NCNT/CNFs)	Pyridine pyrolysis over flexible electrospun carbon nanofibers film (CNFs) with the nano-Fe catalyst	O-7.9, N-4.8 at%	0.1 M KOH	0.91 V, 3.8		94.65%—10 000 s	[151]
Nitrogen-doped carbon foam (CFN)	Combustion of diethanolamine (N) and ethanol (C sol-gel) with resorcinol (R) and formaldehyde-pyrolysis in ammonia—postheating at 800 °C	0.65 at% N	0.1 M KOH	0.92 V, 3.9		94.7% after 60 000 cycles	[152]
N-C xerogel	Silica spheres+GO+ N (cyanamide, melamine and urea)-900 °C	5 at% N	0.1 M NaOH	0.96 V, 3.7		97.7% after 1000 cycles	[153]
N-G foams	GO in ethanol+3-aminopropyltriethoxysilane +900 °C	N-3.15 at%, SA ≈ 918.7 m <sup>2</sup> g <sup>-1</sup>	0.1 M KOH 0.1 M HClO <sub>4</sub>	0.94, 3.9 0.81, 3.8		≈97% after 5000 cycles	[154]
3D N-G	Autoclave of melamine, resorcinol, hexamethylenetetramine, and colloidal silica-(120 °C)-pyrolysis 600–900 °C	2.92%, 913 m <sup>2</sup> g <sup>-1</sup>	0.1 M KOH	0.93 V, 3.7		100% after 800 s	[155]
N-macro/mesoporous C	Pyrolyze-dry bacterial cellulose derived aerogel in N <sub>2</sub> at 800 °C CNF aerogels, heating in NH <sub>3</sub> at 700–900 °C	3.48%, 845 m <sup>2</sup> g <sup>-1</sup>	0.1 M KOH	0.91 V, 4		Small change after 4000 cycles	[156]
N-C nanofiber aerogel		5.8%, SA ≈ 916 m <sup>2</sup> g <sup>-1</sup>	0.1 M KOH 0.5 M H <sub>2</sub> SO <sub>4</sub>	0.85 V, 3.96 0.83 V,		97.5% after 10 000 cycles	[157]

Table 2. Continued.

Material	Synthesis method	Chemical content and property	Electrolyte	Onset potential [V vs RHE] and <i>n</i>	Tafel slope [mV per decade]	Stability	Ref.
N-C nanofiber aerogels	Hydrothermal carbonization—ultrathin tellurium nanowire templated glucosamine hydrochloride at 900 °C; CO <sub>2</sub> activation at 1000 °C	N-1.64 at%, 1324 m <sup>2</sup> g <sup>-1</sup>	0.1 M KOH	0.93 V, 3.74–4.02		87.2% after 15 000 s	[158]
N-C capsules	Glyoxal dispersed in ethanol and melamine, pyrolysis—800 °C	N/C-15, SA = 595 m <sup>2</sup> g <sup>-1</sup>	0.1 M KOH	0.91 V, 3.7		80% after 252 000 s	[159]
N-hole graphene	GO treated in nitric acid (conc.); then solvothermally treated with urea	N-8.6 at%, SA = 784 m <sup>2</sup> g <sup>-1</sup>	0.1 M KOH	0.885 V, 3.85		90% after 10 000 s	[160]
Polymer derived 3D N-C network	Self-assembled polyaniline inside NaCl via recrystallization, pyrolysis	N/C = 3.52 to 3.85%, SA = 265.7 m <sup>2</sup> g <sup>-1</sup>	0.1 M KOH	0.78 V, 3.9			[64]
Porous N-C	<i>o</i> -Phenylenediamine and silica colloid pyrolysis at 900 °C in Ar	N = 3.15 to 9.5 at%, SA = 1280 m <sup>2</sup> g <sup>-1</sup>	0.1 M KOH	≈0.92 V, 2.62 to 3.86		≈98% after 10 000 cycles	[161]
Hierarchical N-C	Sodium alginate and urea pyrolysis	SA = 470.9 m <sup>2</sup> g <sup>-1</sup> , N = 2–8 at%	0.1 M KOH	0.94 V, ≈4	68 mV per decade	81% after 20 000 cycles	[162]
MOF-derived N-C	MOF pyrolysis and NH <sub>3</sub> activation	N = 4.4–5.5 at%, SA = 2412 m <sup>2</sup> g <sup>-1</sup> , D = 6.8 nm	0.1 M KOH 0.5 M H <sub>2</sub> SO <sub>4</sub>	0.96 V, 3.9–4 0.84 V,	53 mV per decade 98 mV per decade	98.33% after 10 000 cycles-	[163]
MOF-derived, porous N-C	Pyrolysis of Mg-MOFs at 1000 °C—1 h	N-1.3 to 5.7 at%, SA = 1500 m <sup>2</sup> g <sup>-1</sup>	0.1 M KOH	0.82–0.915 V, 3.6–3.9			[164]
MOF-derived pyridinic N-C	Autoclave (140 °C)—2,2'-bipyridine-5,5'-dicarboxylate, AlCl <sub>3</sub> ·6H <sub>2</sub> O and acetic acid; pyrolyzed at 100 °C—12 h	N = 7.6 at%, SA 1180 m <sup>2</sup> g <sup>-1</sup>	0.1 M KOH	0.89 V, 3.82		95% after 9000 s	[165]
N-CNT/rGO from polymer	Adhesion of poly( <i>p</i> -phenylenevinylene) (PPV) precursor	N-4.21 at%, SA = 268 m <sup>2</sup> g <sup>-1</sup>	0.1 M KOH	0.92 V, 3.99		92% after 40 000 s	[166]
Graphene sheets inside CNT voids	Annealing FeCl <sub>3</sub> and cyanamide mixture—900 °C in Ar	N-6.6 at%, SA = 363.8 m <sup>2</sup> g <sup>-1</sup>	0.1 M KOH	0.885 V, 3.98		—	[167]
N-porous carbon	Pyrolysis (1000 °C) Resorcinol + formaldehyde + ammonium carbonate-pyrolysis in NH <sub>3</sub> flow	N-3.12 at%, SA = 2986 m <sup>2</sup> g <sup>-1</sup>	0.1 M KOH	0.95 V, 3.75		98.6% after 10 000 cycles	[84]
N-C	Polymerization: melamine–resorcinol–hexamethylenetetramine, pyrolysis at 900 °C in N <sub>2</sub>	N-3.48 at%, SA = 845 m <sup>2</sup> g <sup>-1</sup>	0.1 M KOH	0.91 V, ≈4		98.7% after 4000 cycles	[156]
N-C (coal tar derived)	Coal tar processing and oxidizing in concentrated acids and pyrolyzed at 900 °C	N-3.5 wt%, SA = 1985.1 m <sup>2</sup> g <sup>-1</sup>	0.1 M KOH	0.92 V, >3.8 (0.27–0.85 V)		98.8% after 3000 cycles	[168]
Sponge-like N-C/graphitic-C <sub>3</sub> N <sub>4</sub>	Pyrolysis of C-chitin/g-C <sub>3</sub> N <sub>4</sub> solution with NaOH at 800 °C	N-13.19 at%	0.1 M KOH	0.89 V, 3.9	76 mV per decade	86.8% after 50 000 s	[169]
Mesoporous C <sub>3</sub> N <sub>4</sub> /Carbon	Pyrolysis: silica microspheres with sucrose-900 °C, cyanise at 550 °C	C <sub>3</sub> N <sub>4</sub>	0.1 M KOH	0.84 V, 3	150, 190 mV per decade	≈85% after 60 h	[170]
Porous graphitic C <sub>3</sub> N <sub>4</sub> /carbon composite spheres	Pyrolysis (600 °C) of melamine and cyanuric acid, and glucose mixed	N/C = 0.69, SA = 450 m <sup>2</sup> g <sup>-1</sup>	0.1 M KOH	0.9 V, 3.4		80% after 20 000 s	[171]
C <sub>3</sub> N <sub>4</sub> nanosheets and rGO self-assembly	Pyrolysis—melamine: g-C <sub>3</sub> N <sub>4</sub> , mixture of g-C <sub>3</sub> N <sub>4</sub> and GO with xenon lamp in methanol	SA = 310 m <sup>2</sup> g <sup>-1</sup>	0.1 M KOH	0.85 V, 3.8		93% after 20 000 s	[73]
S-C aerogel/GO composite	C-aerogel/resorcinol–formaldehyde polymer aerogel, S-C aerogel: C aerogel heating at 650 °C and 800 °C in H <sub>2</sub> S for 3 h, GO and aerogel sonication	S-2.5%, 412 m <sup>2</sup> g <sup>-1</sup>	0.1 M KOH	0.829 V, 2–3.9		70% after 1300 cycles	[172]
S-graphene foam	Solvothermal with GO and Na <sub>2</sub> S	S-0.5%, SA = 66 m <sup>2</sup> g <sup>-1</sup>	0.1 M KOH	—	—	≈100%—1000 cycles	[173]

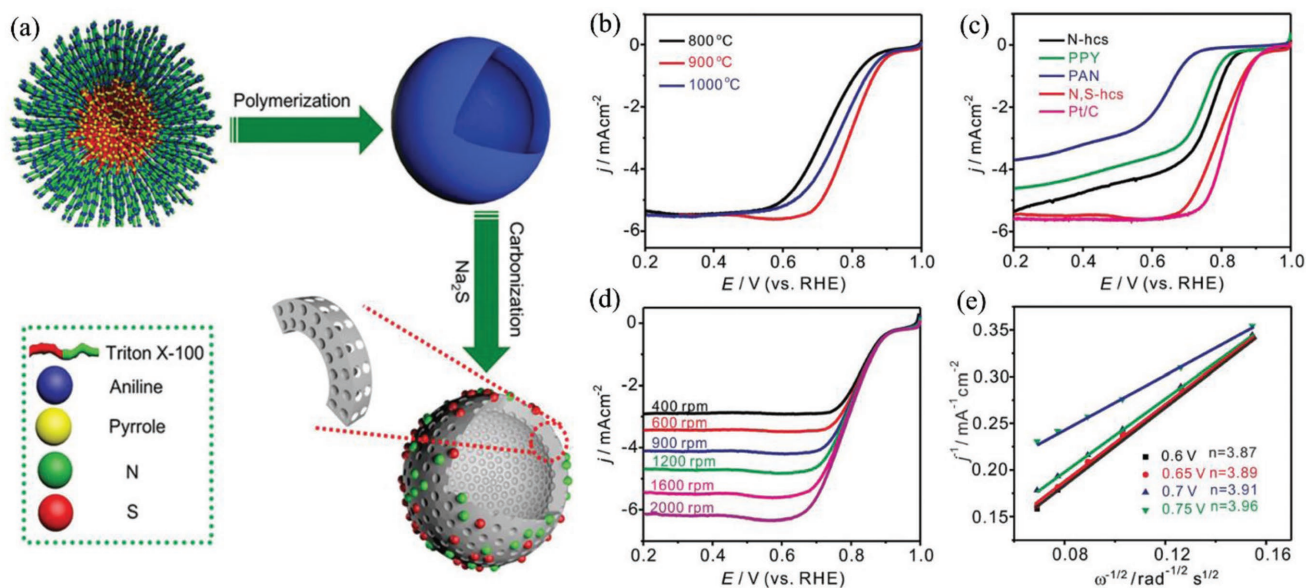


**Figure 5.** a) Schematic for N/S-hcs preparation, b) LSVs of N,S-hcs treated at various temperatures, and c) samples (at 1600 rpm and 5 mV s<sup>-1</sup>). d) LSVs of N,S-hcs-900 °C are at different rotating speeds and e) the Koutecky–Levich curves at different potentials. a–e) Reproduced with permission.<sup>[180]</sup> Copyright 2016, The Royal Society of Chemistry.

Apart from N/S-hcs, various other codoped 3D carbon nanostructures, including N/P-, B/N-, N/F-, and P/C<sub>3</sub>N<sub>4</sub>-codoped hierarchal carbon architectures, have also been fabricated to achieve superior ORR electrocatalytic performance as compared to Pt/C, as summarized in Table 3. Furthermore, three elemental doping (i.e., tridoped) in 3D porous carbon structure has also been studied,<sup>[30,57]</sup> though still not much discussed in the literature as compared with codoping. In particular, N–P–O-tridoped freestanding 3D graphene foam (3D-HPG) has almost isotropic feature, having pores ranging from 50 nm to 1 μm, and exhibited superior ORR catalytic performance of 92% current density retention in alkaline electrolyte with 0.93 V onset potential (vs 81% retention for Pt/C) even after 10 000 s of reaction.<sup>[89]</sup> Density functional theory calculations indicated that N–P–O tridoping is an attractive option for electrocatalysis since it could significantly enhance the charge delocalization.

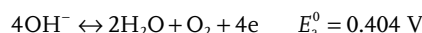
It should be mentioned that structural defects, even without heteroatom doping, have recently recognized to also impart catalytic activities to pure carbon nanomaterials via the so-called defective doping-induced charge redistribution.<sup>[195–199]</sup> Utilizing this concept, graphene nanoribbon supported graphene quantum dots were developed showing ORR performance very closely comparable or superior than the state-of-the-art Pt/C electrode.<sup>[200]</sup> This electrocatalytic excellence may be attributed to the surficial, interfacial, and edge defect sites of quantum dots and graphene nanoribbons, as well as to the efficient charge transfer through their intimate interfaces. Clearly, the quantum defect and interface modification can also be adopted to 3D porous carbon structures with or without heteroatom doping to develop defect-induced ORR electrocatalysis. In this context, biomass-derived 3D porous carbon materials (e.g., chitin, keratin, and shrimp shell)<sup>[201–204]</sup> and D-glucose<sup>[205]</sup> components are also reported to demonstrate as desirable ORR catalytic performance in microbial fuel cells.<sup>[206]</sup>

Clearly, heteroatom-doped 3D carbon structures are superior electrodes for ORR performance due to increase in charge redistribution aided increase in O<sub>2</sub> adsorption and highly abundant active sites in three dimensions. N-doped 3D carbon nanostructured materials have been widely used with a few reports on S-doped carbon structures for ORR applications. Heteroatom-codoped 3D structures are superior to single-doped counterparts as evidenced by many studies. Among them, NS- and NP-codoped 3D mesoporous carbon materials are most efficient for electrocatalysis of ORR and possess potential to replace precious-metal-based catalysts. However, more research is required to clearly understand the influence of structural details of 3D carbon nanostructures on ORR performance. There needs to bring more advancement in acid-electrolyte-based 3D carbon catalysts for commercial success in fuel cell technology.

## 6. 3D Carbon-Based Electrocatalysts for Oxygen Evolution Reaction

Multiple proton–electron-coupled steps that are involved in oxygen evolution reaction to produce molecular oxygen<sup>[207,208]</sup> is pH sensitive. In basic solution, hydroxyl groups (OH<sup>-</sup>) are oxidized into H<sub>2</sub>O and O<sub>2</sub>, whereas in acidic and neutral electrolytes, two adjacent water molecules (H<sub>2</sub>O) are oxidized in four protons (H<sup>+</sup>) and oxygen molecule (O<sub>2</sub>). The equilibrium half-cell potentials ( $E_a^0$ ) at 1 atm and 25 °C for OER are shown as follows:<sup>[209]</sup>

OER in alkaline solution



OER in acidic solution

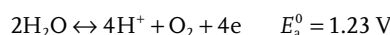


**Table 3.** Doped (co- and tridoped) carbon-based 3D catalysts for ORR.

Material	Synthesis method	Chemical content and property	Electrolyte	Onset potential [V] and <i>n</i>	Tafel slope [mV per decade]	Stability	Ref.
<b>N/S-codoped C</b>							
N/S-G frameworks	Graphene oxide and ammonium thiocyanate/autoclave (180 °C)	N, S 12.3% and 18.4%	0.1 M KOH	0.27 (Ag/AgCl, 3 M), 3.9		85.2% after 20 000 s	[176]
N- and S-codoped micro/mesoporous carbon foams	Templateless and no toxic gas thermal reaction at high temperature (1000 °C) between sulfur sphere core and polyaniline shell	N, S: ≈0.58, 1 at%	0.1 M KOH	0.051 V, 3.67		76.5% after 20 000 s	[177]
N/S C with macroporosity	Monodispersed silica spheres+ 1-methyl-3-propagylimidazolium bromide] [bis(trifluoromethyl)sulfonyl imide+ pyrolysis in N <sub>2</sub> at different temps, SiO <sub>2</sub> remove in HF (1100 °C)	4.4%, 2.6%, 1.1% and 1.0% at 800, 900,1000, and 1100 °C SA = 1146.6 m <sup>2</sup> g <sup>-1</sup> (1100 °C)	0.1 M KOH	-0.11 (Hg/HgO), 3.4 to 3.8 in -0.3 to -0.7 V range		95% after 10 000 s	[178]
Porous S/N-C from honeysuckles	Honeysuckles pyrolysis in N <sub>2</sub> at 600–900 °C	S-0.46%, N-1.75, SA ≈ 246 m <sup>2</sup> g <sup>-1</sup>	0.1 M KOH	0.027 (Hg/HgO), 3.6		Good stability after 1000 cycles	[179]
N/S-doped hollow C sphere	Triton X-100, pyrrole, aniline, ammonium persulfate: pyrolysis	N ≈ 4.2% (wt), S ≈ 3.8% (wt)	0.1 M KOH	0.93 V, 3.9		90% after 20 000 s	[180]
S/N-C aerogel	Glucose and ovalbumin heated in autoclave at 180 °C for 5.5 h; N source: 900 °C pyrolysis in N <sub>2</sub> ; S source: S-(2-thienyl)-L-cysteine (TC) or 2-thienyl-carboxaldehyde (TCA),	N-3.3%, S-0.5%. SA ≈ 224.5 m <sup>2</sup> g <sup>-1</sup>	0.1 M KOH 0.1 M HClO <sub>4</sub>	-0.13 V (Ag/AgCl), 2–4 >0.2 V (Ag/AgCl), 2–4		89% and ≈75% after 12 000 s	[182]
N/S-porous carbon	iron and polyquaternium-2 dispersed onto SiO <sub>2</sub> spheres followed by coagulation, pyrolysis, SiO <sub>2</sub> removal and H <sub>2</sub> SO <sub>4</sub> leaching	N ≈ 3.9% (at), S = 0.76% (at); SA ≈ 1201 m <sup>2</sup> g <sup>-1</sup> , pore, <i>d</i> ≈ 1–28 nm	0.1 M KOH 0.5 M H <sub>2</sub> SO <sub>4</sub>	0.95 (SHE), 3.97 0.8 (SHE), 3.97–3.99		100% and 95.2% after 5000 cycles	[183]
N/S graphene	Self-assembled pyrrole polymerized on graphene oxide template, pyrolysis	≈9.05% (at), S ≈ 1.65% (at)	0.1 M KOH 0.5 M H <sub>2</sub> SO <sub>4</sub>	0.338 (Ag/AgCl), 4 0.73 V, 3.92		78.2, 77.4% after 30000 s	[184]
N/S-porous C/Pt	Ionic liquid (1 butyl 3 methylimidazolium bis(trifluoro methylsulfonyl)imide) (C <sub>10</sub> H <sub>15</sub> F <sub>6</sub> N <sub>3</sub> O <sub>4</sub> S <sub>2</sub> )+KCl+ZnCl <sub>2</sub> pyrolysis at 850 °C	N, S ≈ 7.03, 1.68 at%, SA ≈ 1424 m <sup>2</sup> g <sup>-1</sup>	0.5 M H <sub>2</sub> SO <sub>4</sub>	0.85 (SCE), 4		≈100% after 126 000 s	[185]
N/S-C nanowire aerogel	Hydrothermal synthesis using D-(+)-glucosamine hydrochloride and thiourea, pyrolysis at 900 °C	N-6.38%, S-0.84 at%, SA ≈ 870 m <sup>2</sup> g <sup>-1</sup>	0.1 M KOH	0.905 V, 4.3		91% after 20 000 s	[186]
<b>B/N-codoped C</b>							
N-, B-, B/N-doped 3D G networks	Ni foam template and electrochemical doping		0.1 M KOH	-3.7 (Ag/AgCl), 3.6 and 3.8, respectively.		85%, 70% and 82% after 3000 s	[187]
Hydrogel: B/N-doped porous C network	Pyrolysis of agarose hydrogel containing TBE buffer (boric acid, tris base, and ethylenediaminetetra acetic acid); KOH activation.	B/C ≈ 0.1%, N/C ≈ 0.7%, SA ≈ 2666 m <sup>2</sup> g <sup>-1</sup>	0.1 M KOH	-0.18 (Ag/AgCl), 3.64		95.3% after 10 000 cycles	[88]
B/N-doped graphene aerogel	GO treated with urea and chitosan, then the product pyrolyzed at 1000 °C mixing with boric acid	Pore diameter ≈ 88.3–185.6 nm, SA ≈ 545.7 m <sup>2</sup> g <sup>-1</sup> ,	0.1 M KOH	-0.07 (SCE), 3.87	73 mV per decade	95% after 10 000 s	[188]
h-B/N rGO composite	rGO/BN by hydrothermal method, annealing at 750 °C in N <sub>2</sub>	hBN ≈ 5 wt%	0.1 M KOH	0.798 (Ag/AgCl, Sat.), 3.8		≈95% after 10 000 cycles	[189]
<b>N/P-codoped C</b>							
N/P porous C	copyrolyzing N and P containing precursors + poly(vinyl alcohol)/polystyrene: hydrogel composites	1083 m <sup>2</sup> g <sup>-1</sup>	0.1 M KOH	0.946 (RHE), 3.9–4			[190]
N/P-G nanoribbons/CNT composites	Partially unzipped CNTs and ammonium dihydrogen phosphate (NH <sub>4</sub> H <sub>2</sub> PO <sub>4</sub> ) grounded and annealed 900 °C for 2 h in N <sub>2</sub>	N-0.94% P-2.56%	0.1 M KOH	0.90 (RHE), 3.97	46.7 mV per decade	≈96% after 600 s	[191]
N/P-porous carbon	Melamine+amino trimethylene phosphonic acid+carbon quantum dots, pyrolyzed up to 1000 °C in Ar for 1 h	N-3.48, P-0.91 at%, SA ≈ 743 m <sup>2</sup> g <sup>-1</sup> (900 °C)	0.1 M KOH 0.5 M H <sub>2</sub> SO <sub>4</sub>	0.92 (RHE), 3.89 0.74 (RHE), 3.64		84.2% 73.6% after 12 000 s	[192]

**Table 3.** Continued.

Material	Synthesis method	Chemical content and property	Electrolyte	Onset potential [V] and $n$	Tafel slope [mV per decade]	Stability	Ref.
P/C <sub>3</sub> N <sub>4</sub> nanosheets and -NH <sub>2</sub> -functionalized carbon black composite	Nitrilotris(methylene)-triphosphonic acid with dicyandiamide-thermal polycondensation at 600 °C—addition of NH <sub>2</sub> -CB and freeze-drying	N-42.72, O-6.03 and P-4.53%, SA = 286 m <sup>2</sup> g <sup>-1</sup>	0.1 M KOH	0.87 (Hg/HgO), 3.83	89 mV per decade	≈94% after 3000 cycles	[193]
N/F-codoped C							
N/F-C aerogel	Hydrothermal carbonization of glucose and ammonium fluoride up to 1000 °C in N <sub>2</sub>	N-1.8, F-0.04 at%, SA-768.4 m <sup>2</sup> g <sup>-1</sup>	0.1 M KOH	0.912 (RHE), 3.7	70 mV per decade	95% after 20 000 s	[194]
Tridoped C							
N/P/O-G	Mixture of ball-milled Artemia cyst shells and red P: KOH activation and pyrolysis at 850 °C	O,N,P-9.12, 1.19 and 1.02 at% respect. SA = 1406 m <sup>2</sup> g <sup>-1</sup>	0.1 M KOH	0.928 (RHE), 3.83		92% after 10000 s	[89]
N/S/O hierarchical C sheet with holes	Melamine, nickel sulfate and potassium chloride ball milled and pyrolyzed at 800 °C	N-2.1, S-0.8 and O-3.8 at%, SA = 576 m <sup>2</sup> g <sup>-1</sup>	0.1 M KOH 0.5 M H <sub>2</sub> SO <sub>4</sub>	0.94 V (RHE), 3.85 ≈0.9 V(RHE)		≈95% after 100 h	[30]
N/P/F graphene	Pyrolysis (650 °C) of GO-PANi in ammonium hexafluorophosphate (AHF)	N-7.11, P-0.37 and F-0.33 at%, SA = 512 m <sup>2</sup> g <sup>-1</sup>	0.1 M KOH	≈0.93 (RHE), 3.85		100% after 1.4 h	[57]

In order to maintain the working voltage around 1.23 V and to avoid the pH influence on the applied potential, a reversible hydrogen electrode is usually adapted as reference.<sup>[209]</sup> As it is known, the evolution and transfer of four electrons out of O<sub>2</sub> molecule needs multistep reactions of single electron transfer in each step to achieve favorable kinetics for OER process to take place. Also, sluggishness in OER kinetics is triggered by the energy accumulation at each step, resulting in a huge overpotential. So, to overcome the energy barrier highly active OER electrocatalyst is required.<sup>[210,211]</sup> Consequentially, characteristics of an ideal OER catalyst should be of high catalytic stability

with related low overpotential, low cost, and earth-abundance for large-scale commercialization.

The heteroatom-doped 3D carbon materials and their OER catalytic performance is summarized in **Table 4**. Although N-doped mesoporous carbon showed a better OER catalytic stability,<sup>[204]</sup> N/O-codoped hydrogel<sup>[214]</sup> has shown a lower onset potential (1.28 V) for OER in 0.1 M KOH besides that observed in N-doped porous carbon<sup>[212]</sup> and C<sub>3</sub>N<sub>4</sub>/CNT composite catalysts.<sup>[213]</sup> The (0.5 M H<sub>2</sub>SO<sub>4</sub>) N/O hydrogel exhibited a better OER performance as compared to that in commercial IrO<sub>2</sub> electrode in acid medium.<sup>[214]</sup> In an alkaline medium of (0.1 M KOH) even

**Table 4.** Carbon-based heteroatom-doped 3D catalysts for OER.

Material	Method	Content and property	Electrolyte	Onset potential [RHE] and $n$	Potential at 10 mA cm <sup>-2</sup> [RHE] and Tafel slope [mV per decade]	Stability	Ref.
N-porous C	Pyrolyzed GO and dimethylsulfoxide mixture at 700 °C	N-4.1 at%, SA = 560 m <sup>2</sup> g <sup>-1</sup>	0.1 M KOH	1.52 V, 3.9	1.61 V	≈100% after 20 cycles	[212]
C <sub>3</sub> N <sub>4</sub> /CNT	Low-temperature self-assembled CNTs and g-C <sub>3</sub> N <sub>4</sub> sheets	SA = 149 m <sup>2</sup> g <sup>-1</sup> , N-23.7 wt%	0.1 M KOH	1.53 V, 4	1.6 V, 83	86.7% after 10 h	[213]
N/O-C hydrogel	rGO and CNTs layer-by-layer assembly, autoclaved N-doping with ammonia	N/C-9.9%, SA = 519 m <sup>2</sup> g <sup>-1</sup>	0.1 M KOH 0.5 M H <sub>2</sub> SO <sub>4</sub>	1.28 V, 4 better than IrO <sub>2</sub>	1.7 V, 141 better than IrO <sub>2</sub>	≈80% after 200 cycles	[214]
S/N-C foam	Exfoliated graphite via acid+thiourea, autoclaved 12 h at 180 °C	N, S = 1.18 and 0.51 at%	0.1 M KOH	1.55 V,	0.38 V, 98	77% after 16 h	[215]
S/N-G/CNTs	urea and thiourea treated GO+CNT, autoclaved at 180 °C for 12 h	N-0.71, O-3.1, S-1.26 at%	0.1 M KOH	1.57 V, 4	1.89 V, 103	–	[216]
N/P-doped active C-fiber	Calcined and acid treated C paper+ electrochemical hydrogel growth in aniline and ethylene diphosphonic acid, pyrolysis 2 h at 700 °C	SA = 473 m <sup>2</sup> g <sup>-1</sup>	1 M KOH	1.51 V, 4	1.54 V, 87.4	93.4% after 12 h (IrO <sub>2</sub> = 72.9%)	[217]
P/C <sub>3</sub> N <sub>4</sub> -C fiber	Pyrolysis at 550 °C of hydrothermal treatment of c-paper in melamine+ethylene diphosphonic acidpyrolysis	N-13.2 wt%, P-0.9 wt%	0.1 M KOH	1.53 V,	1.63 V, 61.6	93.4% after 30 h	[218]

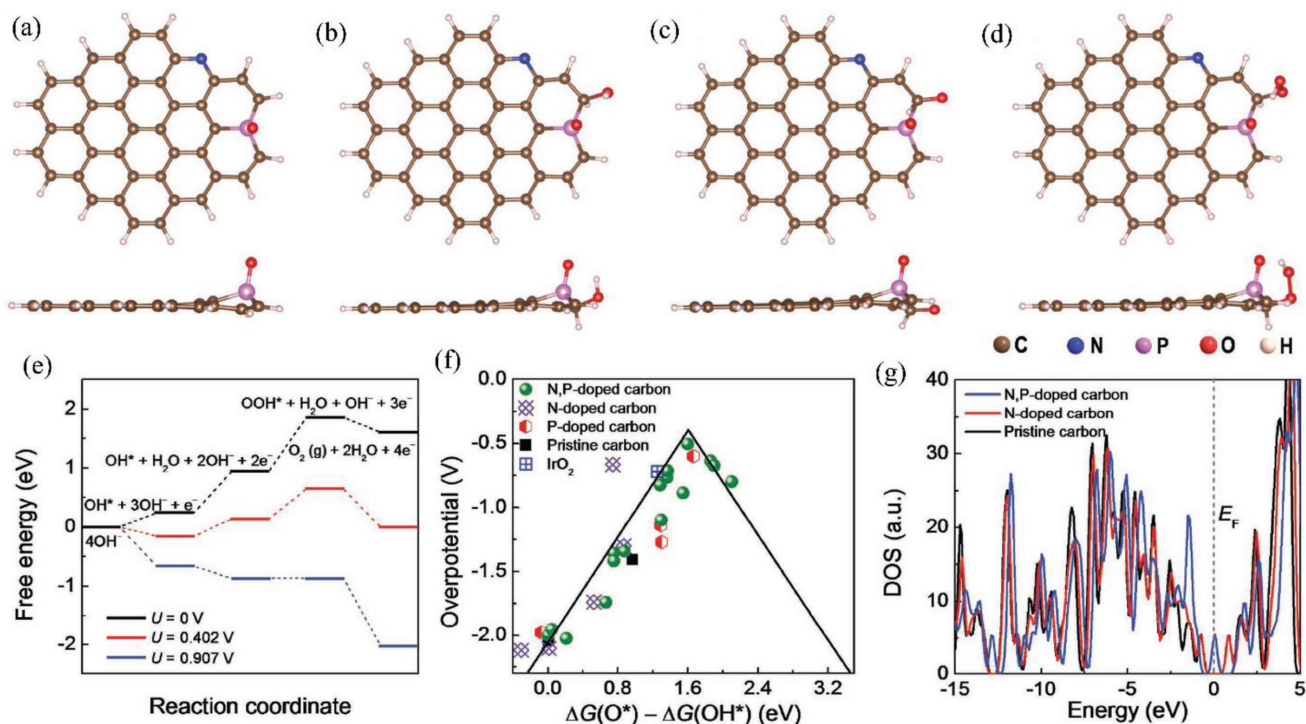


**Figure 6.** Theoretical OER study: atomic structural details of: a) N- and P-codoped carbon and the corresponding modification after adsorption of: b) OH\*, c) O\*, and d) OOH\* intermediates. e) Estimated free energy diagrams for the OER pathways on N/P-codoped carbon lattice at 0 V, 0.402 V (the equilibrium potential), and 0.907 V. f) Volcano plots of OER overpotential for differently doped metal-free and metal-based electrodes versus the of O\* and OH\* adsorption energy difference. g) The electronic density of states (DOS) for the differently doped carbon materials. a–g) Reproduced with permission.<sup>[217]</sup> Copyright 2017, Wiley-VCH.

with a very low doping amount (0.5–1.26 at%), an efficient OER performance was also observed in S/N-codoped foam and rGO/CNT composite electrodes. This is known to be due to the synergistic effects, modification in electronic configuration in the catalysts, and modulation in conducting properties.<sup>[215,216]</sup> However though, the catalytic stability of the S/N-doped electrodes is lower as compared to that of the N- or N/O-doped carbon-based catalysts. As such, 3D carbon catalysts codoped with P/C<sub>3</sub>N<sub>4</sub><sup>[218]</sup> or P/N<sup>[217]</sup> showed an excellent OER stability (>93% current density retention) in alkaline medium (0.1–1 M KOH) for up to 30 h continuous operation. Here, the P and N codoping of the hierarchically porous carbon nanofibers were done by directly growing polymer nanowires on conductive carbon paper through electrochemical polymerization of aniline monomer in presence of phosphonic acid and followed by carbonization.<sup>[216]</sup> The obtained 3D carbon catalyst shown excellent stability (hardly any attenuation in continuous 12 h operation) and high OER performance with a relatively low (0.31 V at 10 mA cm<sup>-2</sup>) overpotential, which is comparatively close to that of iridium oxide (IrO<sub>2</sub>) and the precious benchmark.<sup>[217]</sup>

Experimental investigation has revealed that codoping carbon with P and N led to an increase in active surface area and the density of active sites in comparison to the single doped or pristine carbon-based counterparts. DFT calculations indicate that N and P dopants synergistically coactivate the adjacent C atoms, inducing enhanced activity toward OER.<sup>[217]</sup> This implies that N,P codoping can sufficiently decrease the total free energy for carbon framework as compared to that of pristine or even

single-doped carbon structures. If the potential is reduced to 0 V, the initial three steps, related to the electron transfer on adsorbing HO\*, O\*, and OOH\*, respectively, become endothermic. However, the fourth step remains exothermic which is related to desorption of O<sub>2</sub>. Interestingly, the third step relates to highest reaction energy barrier ultimately controlling the reaction rate-determining step. When the potential is raised close to 0.907 V (i.e., 0.505 V overpotential), all the above-mentioned elementary reaction pathways show downhill and exothermic characteristics triggering the OER to occur spontaneously. **Figure 6** illustrates the initial structure of N,P-codoped carbon lattice (Figure 6a) and related structural modulation after adsorption of OH\* (Figure 6b), O\* (Figure 6c), and OOH\* (Figure 6d) intermediates. The Gibbs free energy diagrams of the OER catalytic reaction pathway on N,P-codoped carbon possessing different potentials infer spontaneous reaction mechanism. Obviously, the electrocatalytic OER overpotential was considerably reduced through heteroatoms codoping. This observation prescribes that OER performance can be well improved by N,P-codoping in carbon structures.<sup>[217]</sup> In fact, the heteroatoms codoping into carbon materials have produced numerous OER electrocatalysts with even multifunctional activities.<sup>[62,90,91,169,218–226]</sup>

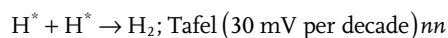
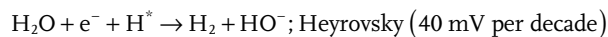
Therefore, SN- and NP-codoped 3D carbon-based electrodes are most efficient for OER electrocatalysis. Particularly, heteroatom (P and S)-doped C<sub>3</sub>N<sub>4</sub>-based porous carbon structures are excellent electrode candidate in this context. Codoping induced enhancement in OER efficiency by 3D carbon catalysts are often attributed to heteroatom induced charge

redistribution and synergistic effects related to doping. There are various parameters related to 3D carbon materials to influence onto OER activities which must be emphasized through more in-depth research studies.

### 7. 3D Porous Carbon-Based Electrocatalysts for Hydrogen Evolution Reaction HER

Although hydrogen's superb emission-free fuel characteristics, hydrogen is mostly generated through steam reforming of natural gas—a process that generates carbon dioxide emissions (also observed in water gas shift reaction).<sup>[227,228]</sup> In contrast, electrochemical process of water reduction can produce H<sub>2</sub> via hydrogen evolution reaction with no environment-degrading emission. However, the high cost of Pt, active electrocatalyst used for most HER, has impeded the large-scale commercial production of H<sub>2</sub> through HER. Hence, it would be very important to develop cost-effective and efficient HER electrocatalysts alternative to Pt. In this context, metal-free electrocatalysts derived from carbon have emerged to be an excellent alternative to Pt since several years. Henceforth, intense research efforts have been devoted in fabricating 2D carbon-based HER electrocatalysts.<sup>[229–232]</sup> The utilization of 3D carbon architectures for HER is a recent addition to this field.<sup>[233–240]</sup> Nevertheless, a few specific heteroatom-doped carbon have recently been demonstrated to exhibit attractive catalytic activity and stability toward HER in neutral, basic, as well as acidic conditions.

There are different mechanisms, Volmer/Heyrovsky/Tafel, for HER as shown below although these holds for other electrochemical reactions, such as ORR and OER as well:<sup>[231]</sup>



The Sabatier principle, most sensitive factor that influences HER rate, is the electrochemical balance between adsorption and desorption, which is, generally presented by a “volcano plot.”<sup>[230–232]</sup> Competing reactions determines HER rate, when the substrate interaction is too slow the Volmer reaction is inhibited, whereas, the Tafel/Heyrovsky reaction is suppressed when it is very strong. Thus, in regulating the HER process it is important in properly selecting interfacial properties between the catalyst and electrolyte layer along with ensuring a well-maintained sorption on the catalyst surface. In this regard, the relative adsorption free energy of the H\* intermediate is used to evaluate HER performance for a catalyst and used as an indicator of the catalytic activity. Related to this, Conway and Tilak<sup>[230]</sup> developed a model for inspecting the underpotential deposition coverage of hydrogen on reaction surface and derived the Tafel slopes associate with various mechanisms. The structural defects and heteroatom induced defects in carbon structures modulate the initial charge distribution to introduce electron accumulation area as the catalytic active site for HER.<sup>[2]</sup> This mechanistic understanding of the carbon-defect enhanced HER is applicable to all graphitic and active carbon structures.

**Table 5** summarizes heteroatom-doped 3D carbon-based catalysts for HER.<sup>[234–240]</sup> Among them, the N-doped plasma

**Table 5.** Heteroatom-doped 3D carbon-based catalysts for hydrogen evolution reaction.

Material	Method	Content and property	Electrolyte	onset potential [V vs RHE]	V at 10 mA cm <sup>-2</sup> and Tafel slope [mV per decade]	Stability	Ref.
Microporous graphitic N–C framework	1,2,4,5-Benzenetetramine tetrahydrochloride condensation reaction with octaketo-tetraphenylene assisted with ZnCl <sub>2</sub>	SA ≈ 928 m <sup>2</sup> g <sup>-1</sup>	0.5 M H <sub>2</sub> SO <sub>4</sub>	–0.26	–0.44, 121	–	[234]
Poly(3,4-dinitrothiophene)/SWCNT composite	Yamamoto polymerization: SWNT+PDNT (41.9%) mixture in DMF, pyrolyzed at 70 °C, and acid wash		1 M H <sub>2</sub> SO <sub>4</sub>	–0.04	–0.12, -		[235]
N-doped, plasma-etched 3D graphene	Hydrothermal treatment of GO+dopamine, 800 °C pyrolysis, 20–30 min Ar plasma etching	N-6.9 at%	0.5 M H <sub>2</sub> SO <sub>4</sub> 1 M KOH	–0.06 –0.14	–0.13, 66 –0.22, 108	both ≈100% after 20 h	[236]
gC <sub>3</sub> N <sub>4</sub> nanoribbon network	Autoclave of g-C <sub>3</sub> N <sub>4</sub> and GO suspended mixture at 180 °C	≈23.74 at%	0.5 M H <sub>2</sub> SO <sub>4</sub>	–0.11	–0.27, 54	≈130% after 15 h	[237]
Porous C <sub>3</sub> N <sub>4</sub> @N–graphene	Cynamide+SiO <sub>2</sub> spheres—hydrothermal treatment, plus GO+NH <sub>4</sub> OH, hydrazine reduction	N-4.6 at%, SA-58 m <sup>2</sup> g <sup>-1</sup>	0.5 M H <sub>2</sub> SO <sub>4</sub>	–0.008	–0.08, 49.1	86.3% after 5000 cycles	[238]
N/P–C nanofiber network	Electropolymerization in phytic acid of aniline (precursor for N and C), then pyrolysis	Electrochemical SA ≈ 325 mF cm <sup>-2</sup>	0.5 M H <sub>2</sub> SO <sub>4</sub>	–0.08	–0.15, 69	≈100% after 2000 cycles	[239]
P graphene–C <sub>3</sub> N <sub>4</sub> hybrid	Pyrolysis of GO+triphenylphosphine, 900 °C, + dicyandiamide lyophilization, pyrolysis at 600 °C	N-42.12, P-2.12 at%, SA-119 m <sup>2</sup> g <sup>-1</sup>	0.5 M H <sub>2</sub> SO <sub>4</sub> 0.5 M KOH	–0.076 –0.62	–0.34, 90-	97.53% after 8.3 h	[240]

etched 3D graphene has shown promising HER performance in acid (0.5 M H<sub>2</sub>SO<sub>4</sub>) electrolytes with −0.06 V (RHE) onset potential.<sup>[236]</sup> For example, C<sub>3</sub>N<sub>4</sub> networks of pristine or heteroatom doping, have been tested for HER in both acid and alkaline media,<sup>[237,238,240]</sup> and the graphitic C<sub>3</sub>N<sub>4</sub> nanoribbon network in 0.5 M H<sub>2</sub>SO<sub>4</sub> electrolyte showed HER onset potential of −0.11 V (RHE) while P-doped graphene and C<sub>3</sub>N<sub>4</sub> composite catalyst exhibited an onset potential of about −0.076 V (RHE).<sup>[237,240]</sup> Also worth to note that porous C<sub>3</sub>N<sub>4</sub> nanolayers composited with N-doped graphene nanosheets revealed the lowest onset potential of −0.008 V (vs 0 mV for Pt/C, vs RHE @ 0.5 mA cm<sup>−2</sup>) in 0.5 M H<sub>2</sub>SO<sub>4</sub> electrolyte with very good durability (negligible activity loss >5000 cycles).<sup>[238]</sup> This is due to the synergistic effects originated from i) 3D conductive graphene network, ii) hierarchical porous structure composition in the hybrid material, and iii) exfoliation of C<sub>3</sub>N<sub>4</sub> into nanosheets and highly dense active sites produced by incorporation of pores on the plane of C<sub>3</sub>N<sub>4</sub> sheets.<sup>[238]</sup> Also, other 3D carbon HER catalysts include poly(3,4-dinitrothiophene)/SWCNT composite<sup>[231]</sup> and N/P-codoped carbon nanofiber network.<sup>[239]</sup>

Heteroatom-doped or codoped 3D carbon materials are promising for efficient HER activities due to the charge transfer induced potential modulation on the electrode surface and high active surface area which facilitate the charge transport as well as mass transfer through the porous 3D network. However, the 3D nanostructure must be highly conductive for superior HER performance. In fact, 3D carbon nanostructures for HER application needs more research attention. Among doped carbon 3D nanomaterials C<sub>3</sub>N<sub>4</sub>-based electrodes doped with P or composited with carbon allotropes have been used for HER electrocatalysis toward efficient water splitting. More research is needed in this respect to replace or even be compared with metal-based HER electrocatalytic performance.

## 8. 3D Carbon-Based Multifunctional Electrocatalysts

Multifunctional electrocatalysts, its inherent flexibility of enabling various redox reactions with significant cost reduction, have attracted focused research attention. In this matter, bifunctional 3D carbon catalysts related to ORR and OER activities is summarized in Table 6. As can be inferred from data in Table 6, chemically and electrochemically synthesized (N, P, C<sub>3</sub>N<sub>4</sub>, and B)-doped and (N-C<sub>3</sub>N<sub>4</sub>, P/C<sub>3</sub>N<sub>4</sub>, P/S, B/N, and N/S)-codoped carbon 3D electrodes exhibited electrocatalytic activities for both ORR and OER.<sup>[62,90,91,169,218–226]</sup> As such, in bifunctional catalysts development, hydrothermal synthesis of N-doped mesoporous carbon nanosheet and MWCNT hybrid composite by pyrolyzing glucose, urea, and CNTs has shown to be an efficient approach.<sup>[220]</sup> The resulting hybrid exhibited notable OER performance showing low onset potential of about 1.50 V versus RHE and an overpotential of only 0.32 V at 10 mA cm<sup>−2</sup> while an onset potential of 0.95 V for ORR with an electron transfer number of 4 in alkaline medium (0.1 M KOH). The observed outstanding bifunctional catalytic activity is attributable to several factors, namely, mesoporous structure for a full exposure of active sites available to high specific surface area (594.1 m<sup>2</sup> g<sup>−1</sup>), high N content (10.7 at%), improved

mass/electron transport, simplistic adsorption/release of oxygen bubbles, and a stable structure.<sup>[220]</sup>

Data in Table 6 reveal that heteroatom-doped C<sub>3</sub>N<sub>4</sub> can exhibit excellent catalytic performance for ORR and OER both, though primarily in alkaline media (KOH). Particularly, P-doped C<sub>3</sub>N<sub>4</sub> nanoflowers produced onto a carbon fiber paper showed onset potential of −0.94 V for ORR and 1.53 V for OER.<sup>[218]</sup> Furthermore, C nanocrystals (P,S-CNS; Figure 7) sandwiched in P/S-codoped C<sub>3</sub>N<sub>4</sub> sponge demonstrated exceptionally high specific surface area (1474 m<sup>2</sup> g<sup>−1</sup>) and higher ORR and OER bifunctional catalytic activities than of Pt/C for ORR and RuO<sub>2</sub> for OER, respectively, in spite of limiting current density and onset potential (Figure 8a–f).<sup>[91]</sup> The resultant electrode exhibited an outstanding durability and suitability as oxygen cathode in rechargeable primary Zn–air batteries. These Zn–air batteries indicated remarkable open-circuit voltage of 1.51 V, excellent discharge peak power density of 198 mW cm<sup>−2</sup>, notably high specific capacity of 830 mAh g<sup>−1</sup>, and robust durability even after 210 h mechanical recharging. An excellent reversibility and durability with favorable small polarization in charge–discharge voltage (0.80 V at 25 mA cm<sup>−2</sup>) have also been reported for the Zn–air battery in three-electrode configuration (Figure 8g–j). DFT investigation reveals that the mechanism behind the exceptional electrocatalytic performance of P,S-CNS is due to the codoping-induced efficient mass/charge transport associated with high conductivity of the C<sub>3</sub>N<sub>4</sub>/C composite.<sup>[91]</sup>

It is obvious that recent rapid development of flexible and wearable electronics requires flexible power sources. However, processing and fabrication of flexible electrode fabrication for ORR and OER operations is still a big challenge.<sup>[90,91,169,218,223–242]</sup> In this context, the flexible and sufficiently large-area 3D mesoporous N-functionalized carbon microtube (NCMT) sponge is very interesting.<sup>[90]</sup> The structure possessed micrometer-scale hollow core with graphitic interconnected pore walls. The NCMT sponge demonstrated very good electrocatalytic ORR and OER performance showing very small potential difference (0.63 V) in between OER (10 mA cm<sup>−2</sup>) and ORR (3 mA cm<sup>−2</sup>) current densities.<sup>[90]</sup> In another effort, a high-temperature pyrolysis method was used by Liu et al. to fabricate nanoporous carbon nanofiber films (abbreviated as, NCNFs). This porous film demonstrated excellent bifunctional catalytic performance for ORR and OER. The corresponding onset potential for ORR was 0.97 V versus RHE with a limiting current Density of 4.7 mA cm<sup>−2</sup> and the OER onset potential was about 1.43 V with a value of 1.84 V at 10 mA cm<sup>−2</sup>. These values are very good as per the metal-free carbon-based multifunctional electrocatalysts. Furthermore, the NCNFs were flexible and have 1249 m<sup>2</sup> g<sup>−1</sup> specific surface area, 147 S m<sup>−1</sup> electrical conductivity, 1.89 MPa tensile strength, and 0.31 GPa tensile modulus. These features made the electrode very attractive together with its excellence as air cathode for flexible, high-performance primary liquid ZABs (with high maximum power density of 185 mW cm<sup>−2</sup> and specific capacity of 626 mAh g<sup>−1</sup>, and energy density of 776 Wh kg<sup>−1</sup>) and also for rechargeable liquid ZABs (tiny charge–discharge voltage gap of ≈0.73 V at 10 mA cm<sup>−2</sup>, high retentivity with an initial round-trip efficiency of 62%, excellent stability (voltage gap increased by ≈0.13 V after 500 cycles), and remarkable energy density



**Table 6.** Heteroatom-doped 3D porous carbon-based catalysts for bifunctional activities or ORR and OER.

Material	Method	Content and property	Electrolyte	onset potential [V vs RHE] and n	V at 10 mA cm <sup>-2</sup> [V] and Tafel slope [mV per decade]	Stability	Ref.
O–C fiber (surface exfoliated)	Edge/defect-rich and O-doped graphene in situ exfoliation on carbon fibers	O-13.9%	0.1 M KOH	ORR 0.76 V, 3.5; OER 1.58 V	OER 1.68 V, -	Stable over 40 000 s	[220]
N-CNT/G composite	CVD-NCNT growth on rGO, aided with ethylene diamine	N-3.9%, SA-175.3 m <sup>2</sup> g <sup>-1</sup>	0.1 M KOH	ORR 0.97 V, 4; OER 1.52 V, -	OER 1.67 V, -	-	[221]
N-mesoporous C-nanosheet/CNT hybrid (N-MCN/CNTs)	Urea and glucose hydrothermal treatment of with MWCNTs, 800 °C pyrolysis in Ar	N-10.7, O-4.2 at%, SA-594.1 m <sup>2</sup> g <sup>-1</sup>	0.1 M KOH	ORR 0.95 V, 4; OER 1.5 V	ORR -, 79 OER 1.55 V, 55	ORR-92.5% (7 h), OER-100% (14 h)	[222]
N–C microtube sponge (flexible)	Pyrolysis of facial 100% cotton at 1000 °C under NH <sub>3</sub> for 1 h	SA ≈ 2358 m <sup>2</sup> g <sup>-1</sup> , C, N, O—93.2, 2 and 4.8 at%	0.1 M KOH	ORR 0.89 V, 4 OER 1.5 V	OER-1.52 V, 246	72.9% after 100 h (Pt/C ≈ 50%)	[90]
N-doped carbon nanonets, g-N-MM-Cnet	TTIP/P123/HCl/H <sub>2</sub> O/ethanol in mixture plus dicyandiamide	SA ≈ 1947 m <sup>2</sup> g <sup>-1</sup>	0.1 M KOH 0.5 M H <sub>2</sub> SO <sub>4</sub>	ORR 0.96 V, 3.9 OER 0.37 V	-, 70 1.6 V, 26		[223]
N–C <sub>3</sub> N <sub>4</sub>	Chitin +NaOH+ urea+ g-C <sub>3</sub> N <sub>4</sub> -stirring, drying, pyrolysis at 800 °C in Ar	N-13.19 at%, SA ≈ 87.19 m <sup>2</sup> g <sup>-1</sup>	0.1 M KOH	ORR 0.86 V, 3.9 OER 1.64 V, -	-, 76 1.68 V, -	89.9% 86.8% after 50 000 s	[169]
P/C <sub>3</sub> N <sub>4</sub> nitride nanoflowers-on flexible carbon-fiber paper	P/gC <sub>3</sub> N <sub>4</sub> directly grown on CFP (PCN-CFP) via 550 °C pyrolysis		0.1 M KOH	ORR 0.94 V, - OER 1.53 V	-, 122.3		[218]
P/S C <sub>3</sub> N <sub>4</sub> sponge sandwich with C nanocrystals	Pyrolysis at 500 °C, freeze-drying	N-41.36, P-1.68 and S-1.59%, SA-1474 m <sup>2</sup> g <sup>-1</sup>	0.1 M KOH	ORR 0.97 V/4 OER 1.26 V	-, 61 (Pt/C 78) 1.56, 64	97.4% after 8000 s	[91]
Heteroatom-doped graphene “Idli”	Microwave heating and 300 °C calcination of heteroatom-doped GO and rice flour	SA ≈ 499 m <sup>2</sup> g <sup>-1</sup>	0.1 M KOH	ORR -0.02 V, - OER 0.29 V	-, 49.83 -, 35.71		[224]
B/N-porous C	Calcination of silicon sphere+methyl violet+boric acid, then 800 °C and pyrolysis	N-7.94, O-9.48 and B-1.51 at%	0.1 M KOH	ORR 0.92 V, 3.83 OER 1.19 V	1.23 V		[225,249]
N/S porous C	Teflon-assisted etching of silica template and simultaneous 1100 °C pyrolysis of sucrose and trithiocyanuric acid	N+S-3.21 and O-3.15 wt%, SA ≈ 830 m <sup>2</sup> g <sup>-1</sup>	0.1 M KOH 0.1 M HClO <sub>4</sub> 0.1 M KOH	ORR 0.94 V, 3.86–3.96 0.88 V, 3.89–3.96 OER 1.66 V	1.69 V		[226]
N/P mesoporous C	Pyrolysis (1000 °C) of polyaniline aerogel synthesized in the presence of phytic acid	N ≈ 3.2, P ≈ 1.1, O ≈ 4.9 at%, SA ≈ 1584 m <sup>2</sup> g <sup>-1</sup>	0.1 M KOH 0.1 M HClO <sub>4</sub> 0.1 M KOH	ORR 0.94 V, 3.85 ORR 0.64 V, 3.8 OER ≈1.3 V	-, 104 1.75 V, -		[241]

(378 Wh kg<sup>-1</sup>).<sup>[242]</sup> No doubt, these flexible Zn–air batteries could be interesting energy supplier while integrated as flexible and wearable systems or devices for various applications.

Along with the advancement of 3D carbon-based as bifunctional catalysts for ORR–OER,<sup>[241,242]</sup> 3D carbon electrocatalysts for ORR–HER or OER–HER operations have recently been under intensive research,<sup>[243–246]</sup> as seen in **Table 7**. Among the 3D porous carbon bifunctional catalysts for HER and OER, carbon fiber–CNT–C<sub>3</sub>N<sub>4</sub> composite and N–P–O-tridoped porous carbon are particularly promising.<sup>[244,246]</sup> **Figure 9** shows the synthesis scheme and electrochemical evaluation for isotropic carbon-based heteroatom-doped metal-free electrolyzer made of C<sub>3</sub>N<sub>4</sub>–CNT–CF and S–C<sub>3</sub>N<sub>4</sub>–CNT–CF as bifunctional catalysts for OER and HER in basic as well as acidic media.<sup>[241]</sup> The rationally designed architecture along with the 3D conducting CNT–CF hierarchy helped to show excellent

charge transport and also facilitated the electrolytic mass transport through the electrode. Also, the high quality dispersion and durability of the layered C<sub>3</sub>N<sub>4</sub> structure enabled the excellent OER electrocatalytic activities (1.52 V onset potential vs RHE in 1 M KOH), and the sulfur doping improved the HER performance of the C<sub>3</sub>N<sub>4</sub>-based electrode with -0.15 V onset potential versus RHE in 0.5 M H<sub>2</sub>SO<sub>4</sub> electrolyte.<sup>[244]</sup> The above attributes thus promote self-supported systems for proficient, cheap and environmental protected water splitting.<sup>[244]</sup> Furthermore, the N–P–O-tridoped carbon-based catalyst performed HER and OER activities both in acid (0.5 M H<sub>2</sub>SO<sub>4</sub>) and alkaline (1 M KOH) medium (Table 7).<sup>[246]</sup> It is worth noting that, compared to bifunctional electrocatalysts, the development of tri/multifunctional carbon catalysts is still in infancy.<sup>[30,57]</sup> 3D heteroatom-doped carbon materials for CO<sub>2</sub><sup>[243–248,250–252]</sup> and H<sub>2</sub>O<sub>2</sub><sup>[253–255]</sup> reduction are also in preliminary stage and needs

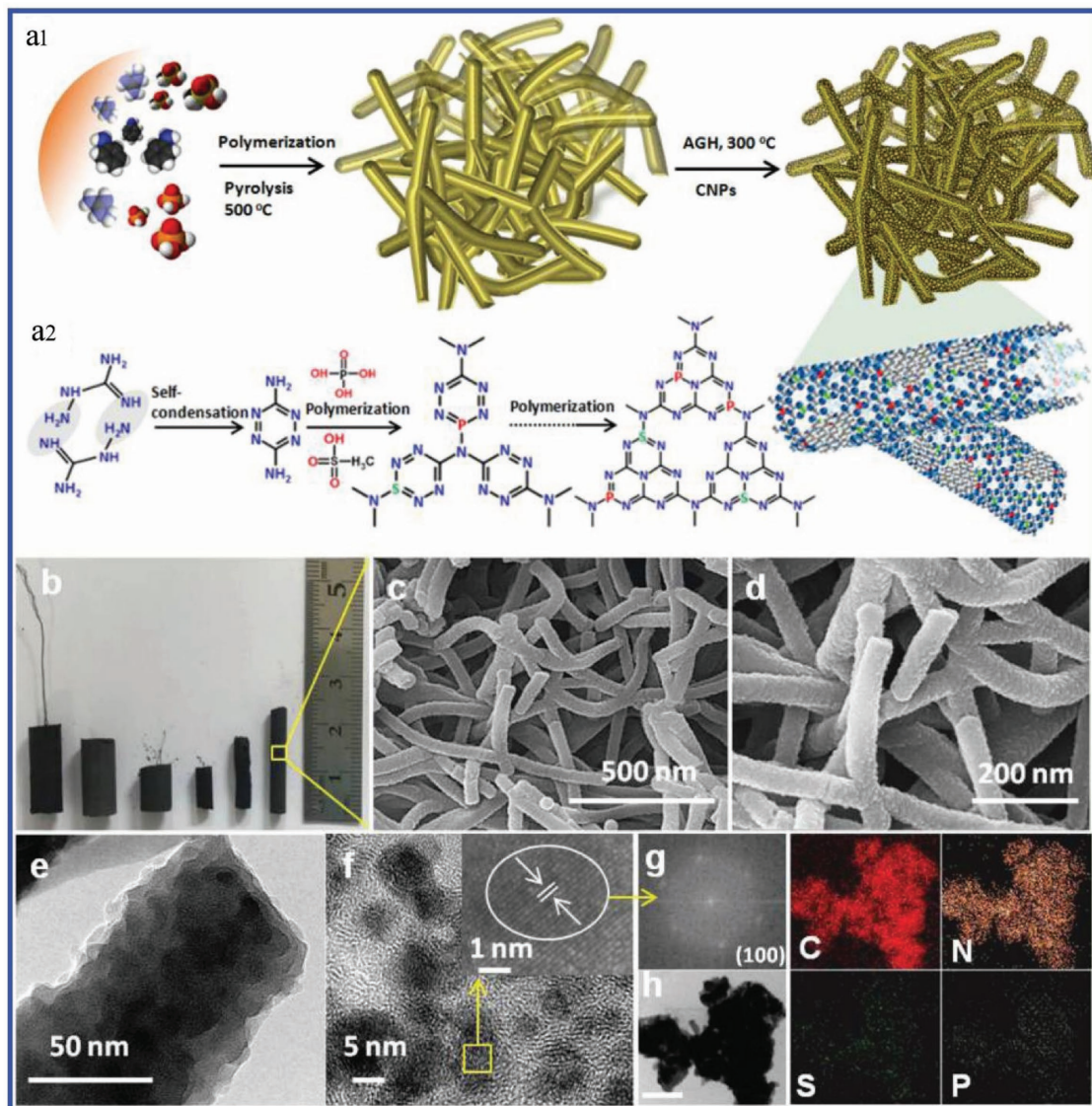


**Figure 7.** a1) Schematic preparation of P,S-CNS catalysts, a2) reaction steps for production of the C–N polymeric complex. b) Digital images of P,S-CNS structure sponge. c,d) SEM, e) TEM, and f) HRTEM images of P,S-CNS nanostructure (inset: zoomed-in view). g) Related FFT pattern for the crystallite structure as shown in the inset of (f). h) TEM and elemental mapping of C, N, P, and S of P,S-CNS (scale, 300 nm). a–h) Reproduced with permission.<sup>[91]</sup> Copyright 2017, American Chemical Society.

considerable attention. Thus, continued research in these emerging areas would be of great value.

3D carbon-based heteroatom-doped have long been applied for bifunctional electrocatalysis in ORR and OER together particularly for metal–air batteries. It is crucial to fabricate innovative electrodes which perform efficiently for both ORR and OER to make commercial impact in this field. Heteroatom-codoped porous carbon materials have demonstrated proficient ORR or OER activity individually and are comparable to metal-based catalysts. However, their bifunctional (ORR and OER) property is often not conclusive. Trifunctional carbon-based efficient catalysts are even more rare. There are few reports on  $C_3N_4$ -based hybrid electrodes and NS- or NP- or NPO-doped 3D carbon materials with efficient ORR, OER, and HER performances.

### 9. 3D Carbon-Material-Based Multifunctional Integrated Energy Devices

Integrated energy systems for simultaneous energy conversion and storage applications have recently received immense technological and commercial interest. Fundamentally, a complete energy system should contain the energy conversion (e.g., solar cells, nanogenerator, among others), energy storage (such as Li-ion batteries, water splitting electrolyzers, supercapacitors, along with others innovative devices), and energy consuming units (e.g., photodetectors, pressure sensors, and magnetic sensors).<sup>[256–262]</sup> Due to technical difficulties in realizing the complex integration and challenges of achieving the low-cost, highly efficient multifunctional catalysts, only a few

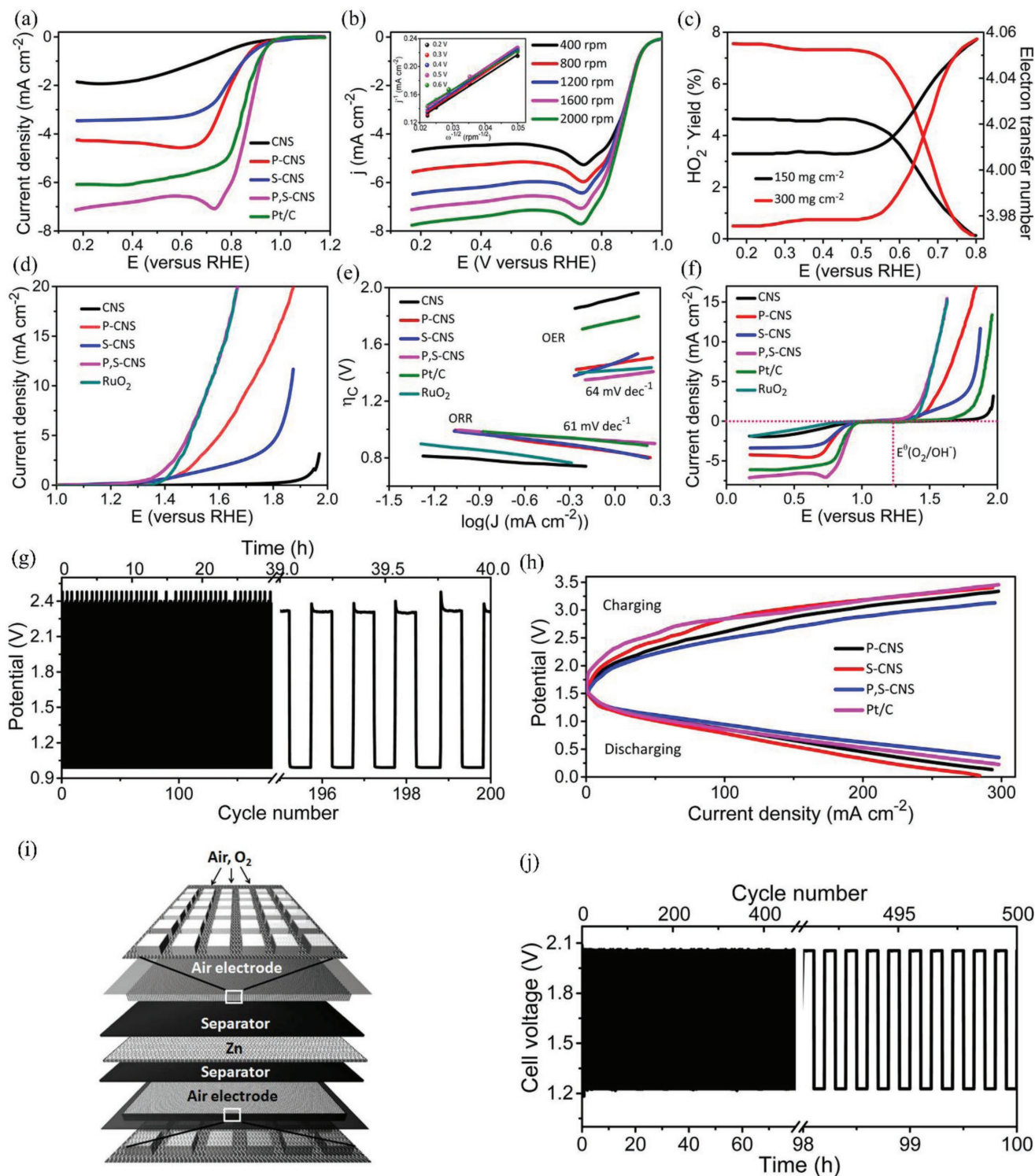


**Figure 8.** a) LSV plots for ORR in  $\text{O}_2$ -saturated 0.1 M KOH medium (1600 rpm). b) LSVs of P,S-CNS of ORR at different rotational speeds; inset: K–L plots at different voltages. c) The  $\text{HO}_2^-$  yield produced in ORR and estimated electron transfer number of P,S-CNS. d) LSVs for OER in 0.1 M KOH electrolyte (1600 rpm). e) Tafel plots of ORR and OER in 0.1 M KOH at 1600 rpm and  $5 \text{ mV s}^{-1}$  scan rate, g) charge–discharge cycles for rechargeable ZABs  $2 \text{ mA cm}^{-2}$  in two electrode configuration with P,S-CNS as air electrocatalyst, h) charge–discharge polarization plots of ZABs in three electrode configuration using commercial Pt/C, P-CNS, S-CNS, and P,S-CNS as air catalysts, i) schematic diagram of trielectrode ZABs, and j) galvanostatic charge–discharge cycles for rechargeable ZABs in three electrode mode using P,S-CNS as bifunctional electrocatalyst. a–j) Reproduced with permission.<sup>[91]</sup> Copyright 2017, American Chemical Society.

**Table 7.** Heteroatom-doped metal-free carbon-based 3D catalysts for trifunctional activities toward ORR, OER, and HER.

Material	Method	Content and property	Electrolyte	onset potential [V vs RHE]	V at 10 mA cm <sup>-2</sup> and Tafel slope [mV per decade]	Stability	Ref.
N-activated C	Pyrolysis of activated C in NH <sub>3</sub> flow at 500 °C for 3 h followed by calcination at 1050 °C for 2 h	N-3.73 at%	0.5 M H <sub>2</sub> SO <sub>4</sub> 0.1 M KOH	HER -0.34 ORR 0.882	0.34, 66 -, 57	≈100% and 90.6% after 20 000 s	[243]
S-C <sub>3</sub> N <sub>4</sub> /CNT/C fiber (HER) C <sub>3</sub> N <sub>4</sub> /CNT/C fiber (OER)	Melamine solution soaking of clean cotton cloth dipped into MWCNT suspension; heating (90 °C), calcined in Ar (550 °C), then heating with S powder (450 °C)	SA-53.7 m <sup>2</sup> g <sup>-1</sup>	0.5 M H <sub>2</sub> SO <sub>4</sub> 1 M KOH	HER -0.15 OER 1.52	0.236, 81.6 1.6, 45	88.3% after 12 h 89.6% after 14 h	[244]
N/P C network	1000 °C pyrolysis of melamine-phytic acid supermolecular aggregate+GO	N ≈ 3 and P = 2.2 at%, SA-375 m <sup>2</sup> g <sup>-1</sup>	0.5 M H <sub>2</sub> SO <sub>4</sub> 0.1 M KOH	HER -0.14 ORR 0.92	-0.16, 89 3.5 e	≈96% after 4 h	[55]
N/P/O-porous C	Acid-oxidized carbon cloth+ailine+phytic acid+ammonium persulfate hydrothermal treatment; 1000 °C pyrolysis for 2 h in N <sub>2</sub>	N-0.46, P-0.32 and O-16.4 at%	1 M KOH 1 M KOH 0.5 M H <sub>2</sub> SO <sub>4</sub>	HER -0.4 OER 1.64 HER -0.33 OER 1.7	-0.45, 154 1.65, 84 -0.39, 109 1.7, 200	≈95%, 5 h ≈97%, 5 h ≈80%, 5 h ≈90%, 5 h	[246]

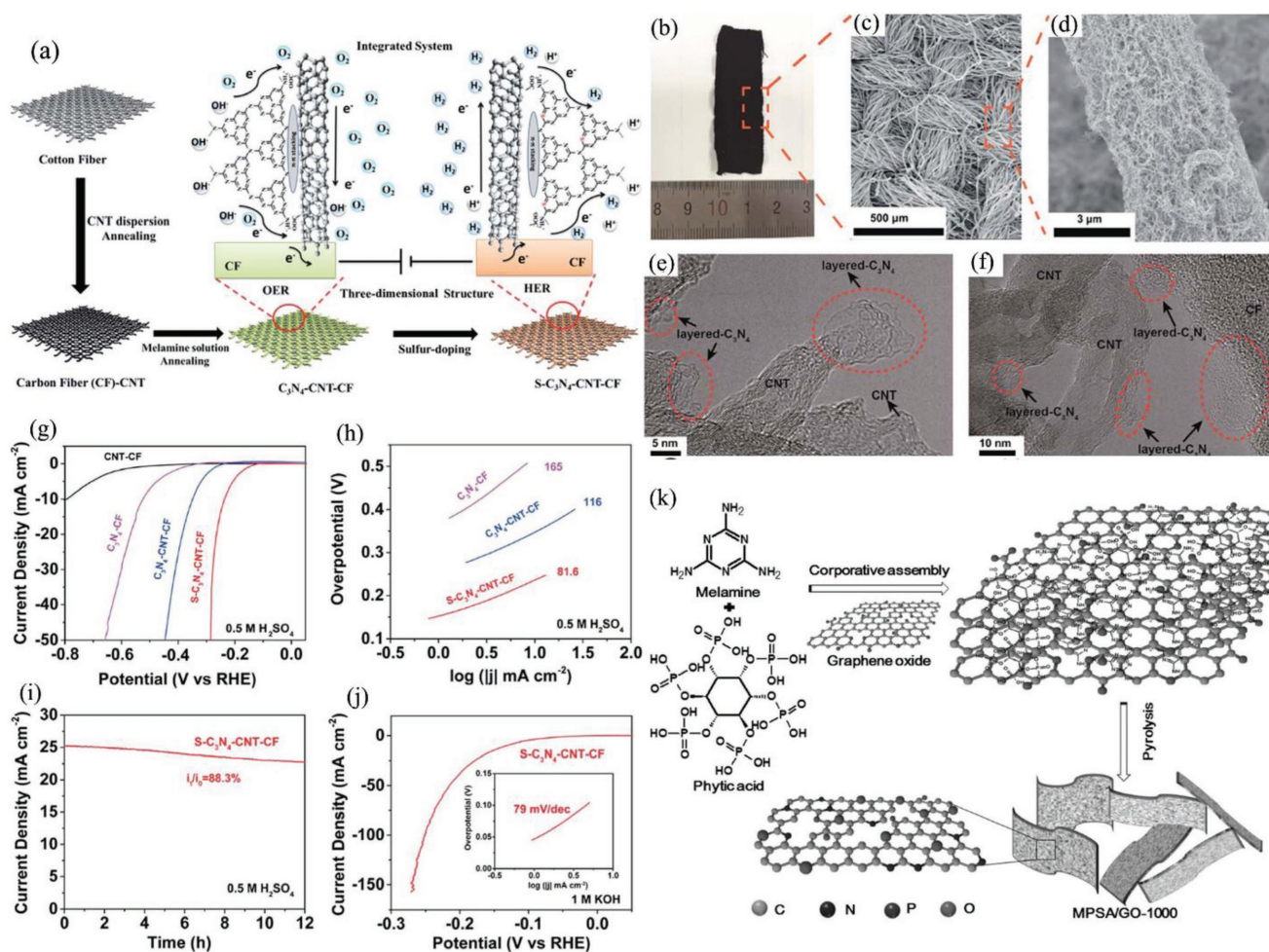


**Figure 9.** a) Schematic preparation process of self-supported C<sub>3</sub>N<sub>4</sub>-based metal-free electrolyzer, b) digital photograph, c, d) SEM images and e, f) HRTEM images of the C<sub>3</sub>N<sub>4</sub>-CNT-CF electrode, g) LSV and h) Tafel plots of CNT-CF, C<sub>3</sub>N<sub>4</sub>-CF, C<sub>3</sub>N<sub>4</sub>-CNT-CF, S-C<sub>3</sub>N<sub>4</sub>-CNT-CF and Pt in 0.5 M H<sub>2</sub>SO<sub>4</sub> at 5 mV s<sup>-1</sup>. i) Chronopotentiometric response of S-C<sub>3</sub>N<sub>4</sub>-CNT-CF in 0.5 M H<sub>2</sub>SO<sub>4</sub>. j) LSV curve of S-C<sub>3</sub>N<sub>4</sub>-CNT-CF in 1 M KOH at 5 mV s<sup>-1</sup> (inset shows the Tafel slope). a–j) Reproduced with permission.<sup>[160]</sup> Copyright 2016, The Royal Society of Chemistry. k) Preparation steps of melamine-phytic acid supermolecular aggregate, MPSA)/GO-1000 through cooperative assemble along with pyrolysis. Reproduced with permission.<sup>[55]</sup> Copyright 2016, Wiley-VCH.

simple integrated energy storage devices have been realized for simultaneous energy conversion and energy storage, and/or as a power source for other electronic devices, such as photodetectors and sensors.<sup>[261–271]</sup> Heteroatom-doped porous carbon materials have recently emerged as building blocks for efficient integrated energy systems and replace the expensive and scarce precious metal and other metal-oxide-based electrodes.<sup>[265,266]</sup>

A wire-shaped integrated energy conversion and storage device was fabricated after twisting two fiber-based electrodes.<sup>[270]</sup> One of the electrodes was composed of titanium oxide nanotube modified titanium wire and the other electrode was made of a fiber fabricated with multiwalled carbon nanotubes and the electrolyte was prepared by incorporating an  $I_3^-/I^-$  redox ion couple into a redox element.<sup>[270]</sup> This wire-shaped

device performed as an efficient dye-sensitized solar cell with 6.58% energy conversion efficiency of 6.58% along with  $85.03 \mu F cm^{-1}$  or  $2.13 mF cm^{-2}$  specific capacitance. Furthermore, the two functionalities could be altered successively without sacrificing performance.<sup>[270]</sup>

In another report, all solid-state and efficient self-powered “energy fiber” was fabricated, which could simultaneously convert solar energy to electric power and store it.<sup>[271]</sup> This opens up a new paradigm for advancement in photoelectronics and electronics technologies. MWCNT sheet was used for wrapping up a modified Ti wire to fabricate the PC panel, as illustrated in Figure 10a–e.<sup>[271]</sup> For the ES panel, poly(vinyl alcohol) (PVA)/ $H_3PO_4$  gel electrolyte was applied onto the titania nanotube-modified Ti wire, and MWCNT sheets were mounted to make

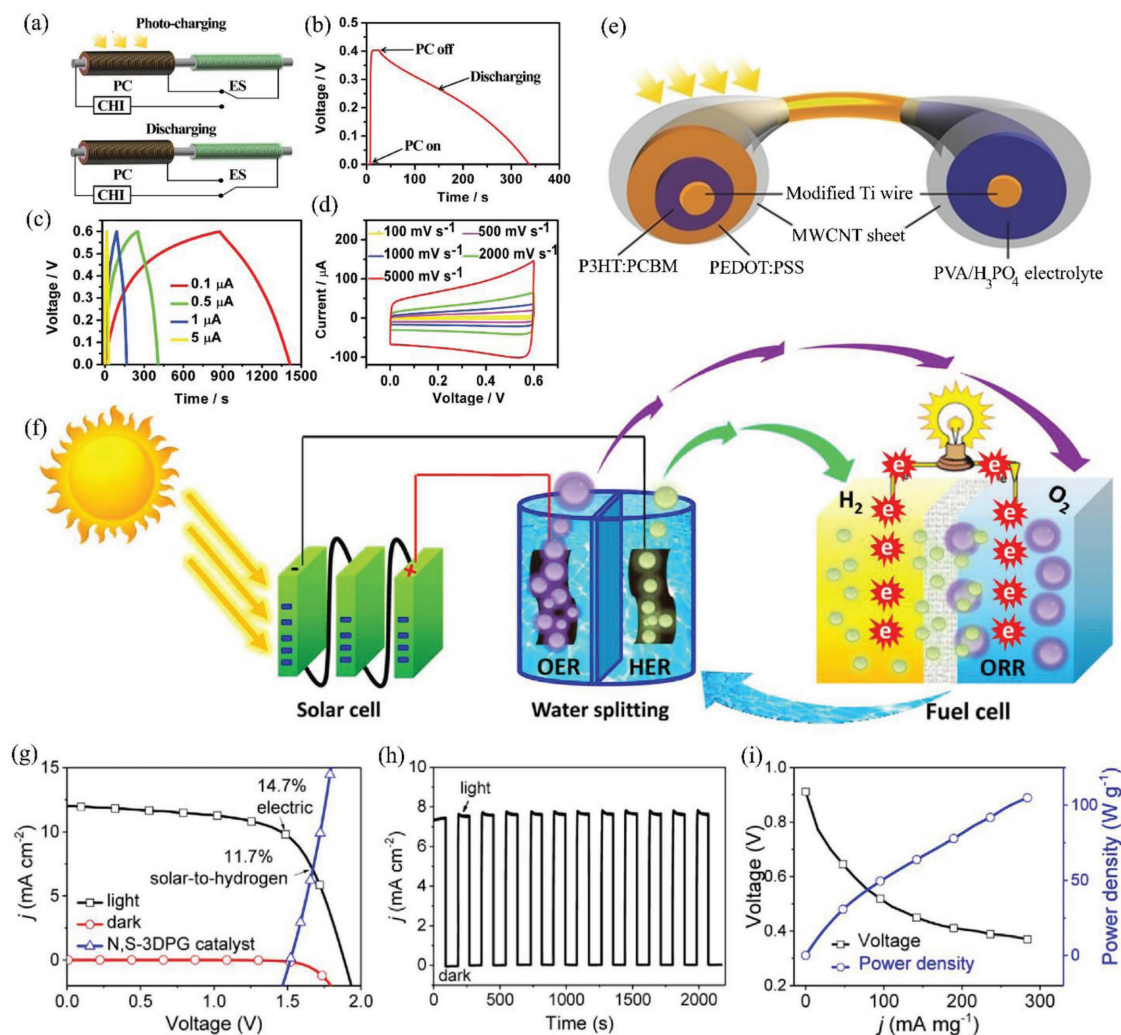


**Figure 10.** Integrated polymer solar cell and electrochemical supercapacitor characteristics in flexible and stable fiber form: a) schematics of the circuit diagram b) charge–discharge characteristics at  $0.1 \mu A$  current during discharge step, c) charge–discharge plots for the self-charged fiber at  $0.1, 0.5, 1$  to  $5 \mu A$  current densities, d) cyclic voltammograms at  $100$ – $5000 mV s^{-1}$  scan rates, e) schematic representation of integrated, all-solid-state, coaxial fiber device (left and right panels are PC and ES, respectively). a–e) Reproduced with permission.<sup>[271]</sup> Copyright 2013, Wiley-VCH. Integrated perovskite cells with water splitting electrolyzer and a fuel cell: f) Schematic demonstration of the multifunctional hybrid system, g) current density versus voltage ( $J$ – $V$ ) characteristics of the perovskite tandem cell for dark and  $100 mW cm^{-2}$  light exposure. h)  $J$ – $t$  characteristics showing the stability and retentivity of the energy conversion performance of integrated water splitting device with on external bias under  $100 mW cm^{-2}$  illumination. i) Gravimetric polarization curve and power density profile with current density of the integrated fuel cell using  $H_2$  and  $O_2$  collected from water splitting electrolyzer operated by the perovskite tandem cells. f–i) Reproduced with permission.<sup>[269]</sup> Copyright 2017, Elsevier Inc.

the ES panel (Figure 10f–i).<sup>[271]</sup> The energy density obtained was  $1.61 \times 10^{-7}$  Wh cm<sup>-2</sup> and the photoconversion and storage efficiency is found to depend on the thickness of MWCNT sheet in ES panel with a maximum value of 0.82% for 20 μm thick MWCNT layer and remained unchanged with further increase in thickness.<sup>[265]</sup> Furthermore, aqueous solar battery was also reported for directly converting solar energy and store as electrochemical energy in carbon nitride structures.<sup>[266]</sup>

Recently, N,S-codoped 3D graphitic framework (N,S-3DPG) was utilized to fabricate cost-effective, high efficient, trifunctional electrocatalyst for HER, OER, and ORR altogether. This technique combines simultaneous HER to produce H<sub>2</sub> fuel through photo-electrochemical splitting of water, OER for O<sub>2</sub> generation from water, and ORR toward clean electricity production in a fuel cell using the H<sub>2</sub> and O<sub>2</sub> gases obtained from HER and OER processes, respectively.<sup>[269]</sup> This multifunctional catalyst, performed light assisted electrochemical water splitting which was operated by CH<sub>3</sub>NH<sub>3</sub>PbI<sub>3</sub> perovskite solar cells and generated clean energy in the form of electricity utilizing the obtained O<sub>2</sub> and H<sub>2</sub> gases in a H<sub>2</sub>-O<sub>2</sub> fuel cell. Figure 10j shows the detailed mechanism of solar energy conversion and storage while Figure 10k–m presents the overall performance of the integrated energy system. The quantum efficiency of the solar cell itself was about 14.7%. The operational current density of the integrated device (Figure 10k) was 7.3 mA cm<sup>-2</sup>, which relates to 11.7% solar-to-hydrogen efficiency (Figure 10l).<sup>[269]</sup> Undoubtedly, such innovative efforts using metal-free carbon catalysts open new avenues for cheap, environmentally protected and storage-free strategy for renewable production of clean energy, although more research is required for further optimization of critical parameters toward a commercial breakthrough for an energy sufficient future.<sup>[272]</sup>

## 10. Conclusions and Perspectives

To make a commercial impact in the field of electrocatalytic chemical energy storage and conversion, the costly metal and metal-oxide-based catalysts must be replaced by cost-effective, but highly efficient, alternatives, due to their low density, high specific surface area, excellent transport properties (both electrical and thermal), and suitable mechanical characteristics. 3D hierarchical mesoporous heteroatom-doped carbon nanostructures have evolved as promising metal-free catalysts to efficiently convert and store energy in various forms. 3D carbon-based hierarchical materials are generally synthesized by a chemical method or chemical vapor deposition techniques. The chemical method is cheaper and can prepare large quantity of electrode materials as compared to the CVD technique. However, 3D carbon materials fabricated by the chemical method are often inferior in structural homogeneity and intrinsic conducting properties. On the other hand, synthesizing actual 3D carbon structures with structural homogeneity is still challenging. Therefore, more attention is required in preparing high-quality 3D carbon electrodes through CVD methods. In this regard, the 3D-printed technique seems very promising approach as an alternative. The activity of the heteroatom-doped 3D carbon electrodes depends on their fabrication and activation techniques.

Furthermore, codoping or even tridoping of 3D mesoporous carbon materials led to multifunctional catalysts with similar or even better electrocatalytic performance than most of the precious metal and other transition-metal-oxide-based electrodes, opening up a new paradigm toward commercialization of renewable energy technologies. However, the debates on the origin of electrocatalytic activity continues, especially regarding the recent advances in single-atom catalysts.<sup>[273–276]</sup> A trace amount of metal impurity can be present in carbon-based electrodes that are perceived as being metal-free catalyst. Researchers must be careful in this regard. Moreover, in-depth studies are undoubtedly required to enlighten the real mechanism to achieve ideally excellent electrode with multifunctional (ORR, OER, and HER) activities. This insight can make advancement in the carbon-based metal-free electrocatalysis for various energy storage and conversion applications. Conclusively, it can be noted that more research efforts are required to utilize 3D heteroatom-doped mesoporous carbon electrodes for integrating various electrochemical energy conversion systems with solar, thermal, mechanical, as well as other electrochemical energy storage systems for efficient, self-powered, and energy sufficient future.

## Acknowledgements

This work was financially supported by the U.S. Air Force Office of Scientific Research (FA9550-12-1-0037), NASA (NNX16AD48A), The National Key Research and Development Program of China (2017YFA0206500), and The National Natural Science Foundation of China (51732002 and 21620102007). The authors would like to thank NSF, NASA, and the Department of Defense-Multidisciplinary University Research Initiative (MURI) for financial assistance. Many thanks are also due to our colleagues, collaborators, and peers for their work cited in this article.

## Conflict of Interest

The authors declare no conflict of interest.

## Keywords

3D heteroatoms, energy devices, metal-free catalysts, nanoporous carbon

Received: August 28, 2018

Revised: November 25, 2018

Published online:

- [1] V. Georgakilas, J. A. Perman, J. Tucek, R. Zboril, *Chem. Rev.* **2015**, *115*, 4744.
- [2] X. Liu, L. Dai, *Nat. Rev. Mater.* **2016**, *1*, 16064.
- [3] L. Dai, Y. Xue, L. Qu, H. J. Choi, J. B. Baek, *Chem. Rev.* **2015**, *115*, 4823.
- [4] Y. Chen, L. Dai, Y. Ohno, *Carbon* **2018**, *126*, 621.
- [5] Z. Xiang, Q. Dai, J. Chen, L. Dai, *Adv. Mater.* **2016**, *28*, 6253.
- [6] A. Erdemir, G. Ramirez, O. L. Eryilmaz, B. Narayanan, Y. Liao, G. Kamath, S. K. R. S. Sankaranarayanan, *Nature* **2016**, *536*, 67.
- [7] R. Paul, *Nano-Struct. Nano-Objects* **2017**, *10*, 69.

- [8] I. Vlasov, O. I. Lebedev, V. G. Ralchenko, E. Goovaerts, G. Bertoni, G. V. Tendeloo, V. I. Konov, *Adv. Mater.* **2007**, *19*, 4058.
- [9] J. Xiao, G. Ouyang, P. Liu, C. X. Wang, G. W. Yang, *Nano Lett.* **2014**, *14*, 3645.
- [10] J. T. Kim, U. Choudhury, H. H. Jeong, P. Fischer, *Adv. Mater.* **2017**, *29*, 1701024.
- [11] R. Paul, A. A. Voevodin, D. Zemlyanov, A. K. Roy, T. S. Fisher, *Adv. Funct. Mater.* **2012**, *22*, 3682.
- [12] H. W. Kroto, J. R. Heath, S. C. O'Brien, R. F. Curl, R. E. Smalley, *Nature* **1985**, *318*, 162.
- [13] W. Kratschmer, L. D. Lamb, K. Fostiropoulos, D. R. Huffman, *Nature* **1990**, *347*, 354.
- [14] S. Iijima, *Nature* **1991**, *354*, 56.
- [15] S. Iijima, T. Ichihashi, *Nature* **1993**, *363*, 603.
- [16] X. Chen, R. Paul, L. Dai, *Natl. Sci. Rev.* **2017**, *4*, 453.
- [17] R. Paul, V. Etacheri, V. G. Pol, J. Hu, T. S. Fisher, *RSC Adv.* **2016**, *6*, 79734.
- [18] H. Tetsuka, A. Nagoya, T. Fukusumi, T. Matsui, *Adv. Mater.* **2016**, *28*, 4632.
- [19] X. Miao, D. Qu, D. Yang, B. Nie, Y. Zhao, H. Fan, Z. Sun, *Adv. Mater.* **2018**, *30*, 1704740.
- [20] J. Mao, J. Iocozzia, J. Huang, K. Meng, Y. Lai, Z. Lin, *Energy Environ. Sci.* **2018**, *11*, 772.
- [21] Y. Wang, Y. Pan, L. Zhu, N. Guo, R. Wang, Z. Zhang, S. Qiu, *Inorg. Chem. Front.* **2018**, *5*, 656.
- [22] X. Gui, Z. Zeng, Y. Zhu, H. Li, Z. Lin, Q. Gan, R. Xiang, A. Cao, Z. Tang, *Adv. Mater.* **2014**, *26*, 1248.
- [23] R. Paul, L. Dai, *Compos. Interfaces* **2018**, *25*, 539.
- [24] H. Wang, X. B. Li, L. Gao, H. L. Wu, J. Yang, L. Cai, T. B. Ma, C. H. Tung, L. Z. Wu, G. Yu, *Angew. Chem.* **2018**, *130*, 198.
- [25] J. Han, D. Kong, W. Lv, D. M. Tang, D. Han, C. Zhang, D. Liu, Z. Xiao, X. Zhang, J. Xiao, X. He, F. C. Hsia, C. Zhang, Y. Tao, D. Golberg, F. Kang, L. Zhi, Q. H. Yang, *Nat. Commun.* **2018**, *9*, 402.
- [26] B. Qiu, M. Xing, J. Zhang, *Chem. Soc. Rev.* **2018**, *47*, 2165.
- [27] X. Li, L. Zhi, *Chem. Soc. Rev.* **2018**, *47*, 3189.
- [28] T. Lv, M. Liu, D. Zhu, L. Gan, T. Chen, *Adv. Mater.* **2018**, *30*, 1705489.
- [29] Y. Xue, Y. Ding, J. Niu, Z. Xia, A. Roy, H. Chen, J. Qu, Z. L. Wang, L. Dai, *Sci. Adv.* **2015**, *1*, e1400198.
- [30] C. Hu, L. Dai, *Adv. Mater.* **2017**, *29*, 1604942.
- [31] Y. He, B. Matthews, J. Wang, L. Song, X. Wang, G. Wu, *J. Mater. Chem. A* **2018**, *6*, 735.
- [32] J. Shi, Y. Dong, T. Fisher, X. Ruan, *J. Appl. Phys.* **2015**, *118*, 044302.
- [33] K. Shehzad, Y. Xu, C. Gao, X. Duan, *Chem. Soc. Rev.* **2016**, *45*, 5541.
- [34] Z. Y. Wu, H. W. Liang, L. F. Chen, B. C. Hu, S. H. Yu, *Acc. Chem. Res.* **2016**, *49*, 96.
- [35] J. Zhang, F. Zhao, Z. Zhang, N. Chen, L. Qu, *Nanoscale* **2013**, *5*, 3112.
- [36] D. C. Marcano, D. V. Kosynkin, J. M. Berlin, A. Sinitskii, Z. Sun, A. Slesarev, L. B. Alemany, W. Lu, J. M. Tour, *ACS Nano* **2010**, *4*, 4806.
- [37] R. Paul, R. N. Gayen, S. Biswas, S. V. Bhat, R. Bhunia, *RSC Adv.* **2016**, *6*, 61661.
- [38] Y. Zhu, L. Peng, Z. Fang, C. Yan, X. Zhang, G. Yu, *Adv. Mater.* **2018**, *30*, 1706347.
- [39] W. Lv, Z. Li, Y. Deng, Q. H. Yang, F. Kang, *Energy Storage Mater.* **2016**, *2*, 107.
- [40] Y. Wang, Z. Wang, *J. Mater. Res.* **2018**, *33*, 1058.
- [41] M. Shao, Q. Chang, J. P. Dodelet, R. Chenitz, *Chem. Rev.* **2016**, *116*, 3594.
- [42] J. Wu, Y. Xue, X. Yan, W. Yan, Q. Cheng, Y. Xie, *Nano Res.* **2012**, *5*, 521.
- [43] T. Ohmori, H. Takahashi, H. Mametsuka, E. Suzuki, *Phys. Chem. Chem. Phys.* **2000**, *2*, 3519.
- [44] M. W. Kanan, D. G. Nocera, *Science* **2008**, *321*, 1072.
- [45] A. Goux, T. Pauporte, D. Lincot, *Electrochim. Acta* **2006**, *51*, 3168.
- [46] J. A. Seaboldand, K. S. Choi, *Chem. Mater.* **2011**, *23*, 1105.
- [47] X. Li, F. C. Walsh, D. Pletcher, *Phys. Chem. Chem. Phys.* **2011**, *13*, 1162.
- [48] L. Dai, *Curr. Opin. Electrochem.* **2017**, *4*, 18.
- [49] K. Gong, F. Du, Z. Xia, M. Durstock, L. Dai, *Science* **2009**, *323*, 760.
- [50] J. Shui, M. Wang, F. Du, L. Dai, *Sci. Adv.* **2015**, *1*, e1400129.
- [51] Y. Zhao, R. Nakamura, K. Kamiya, S. Nakanishi, K. Hashimoto, *Nat. Commun.* **2013**, *4*, 2390.
- [52] J. T. Zhang, Z. H. Zhao, Z. H. Xia, L. Dai, *Nat. Nanotechnol.* **2015**, *10*, 444.
- [53] Y. Zheng, Y. Jiao, L. H. Li, T. Xing, Y. Chen, M. Jaroniec, S. Z. Qiao, *ACS Nano* **2014**, *8*, 5290.
- [54] J. Liu, Y. Liu, N. Liu, Y. Han, X. Zhang, H. Huang, Y. Lifshitz, S. T. Lee, J. Zhong, Z. Kang, *Science* **2015**, *347*, 970.
- [55] J. Zhang, L. Qu, G. Shi, J. Liu, J. Chen, L. Dai, *Angew. Chem., Int. Ed.* **2016**, *55*, 2230.
- [56] B. Kumar, M. Asadi, D. Pisasale, S. S. Ray, B. A. Rosen, R. Haasch, J. Abiade, A. L. Yarin, A. S. Khojin, *Nat. Commun.* **2013**, *4*, 2189.
- [57] J. Zhang, L. Dai, *Angew. Chem., Int. Ed.* **2016**, *55*, 13296.
- [58] B. Men, Y. Sun, M. Li, C. Hu, M. Zhang, L. Wang, Y. Tang, Y. Chen, P. Wan, J. Pan, *ACS Appl. Mater. Interfaces* **2016**, *8*, 1415.
- [59] Z. Lin, G. H. Waller, Y. Liu, M. Liu, C. Wong, *Nano Energy* **2013**, *2*, 241.
- [60] R. L. Liu, D. Q. Wu, X. L. Feng, K. Mullen, *Angew. Chem., Int. Ed.* **2010**, *49*, 2565.
- [61] L. Chen, R. Du, J. Zhu, Y. Mao, C. Xue, N. Zhang, Y. Hou, J. Zhang, T. Yi, *Small* **2015**, *11*, 1423.
- [62] H. Jin, H. Zhang, H. Zhong, J. Zhang, *Energy Environ. Sci.* **2011**, *4*, 3389.
- [63] Y. Ito, H. J. Qiu, T. Fujita, Y. Tanabe, K. Tanigaki, M. Chen, *Adv. Mater.* **2014**, *26*, 4145.
- [64] W. Ding, L. Li, K. Xiong, Y. Wang, W. Li, Y. Nie, S. Chen, X. Qi, Z. Wei, *J. Am. Chem. Soc.* **2015**, *137*, 5414.
- [65] Z. Wen, S. Ci, Y. Hou, J. Chen, *Angew. Chem.* **2014**, *126*, 6614.
- [66] H. B. Yang, J. Miao, S. F. Hung, J. Chen, H. B. Tao, X. Wang, L. Zhang, R. Chen, J. Gao, H. M. Chen, L. Dai, B. Liu, *Sci. Adv.* **2016**, *2*, e1501122.
- [67] Y. Zheng, Y. Jiao, J. Chen, J. Liu, J. Liang, A. Du, W. Zhang, Z. Zhu, S. C. Smith, M. Jaroniec, G. Q. Lu, S. Z. Qiao, *J. Am. Chem. Soc.* **2011**, *133*, 20116.
- [68] M. Zhang, Q. Dai, H. Zheng, M. Chen, L. Dai, *Adv. Mater.* **2018**, *30*, 10.
- [69] L. L. Zhang, X. Zhao, H. Ji, M. D. Stoller, L. Lai, S. Murali, S. McDonnell, B. Cleveger, R. M. Wallace, R. S. Ruoff, *Energy Environ. Sci.* **2012**, *5*, 9618.
- [70] S. N. Faisal, E. Haque, N. Noorbehesht, W. Zhang, A. T. Harris, T. L. Church, A. I. Minett, *RSC Adv.* **2017**, *7*, 17950.
- [71] S. Yang, X. Feng, X. Wang, K. Mullen, *Angew. Chem., Int. Ed.* **2011**, *50*, 5339.
- [72] J. Wu, L. Ma, R. M. Yadav, Y. Yang, X. Zhang, R. Vajtai, J. Lou, P. M. Ajayan, *ACS Appl. Mater. Interfaces* **2015**, *7*, 14763.
- [73] J. Tian, R. Ning, Q. Liu, A. M. Asiri, A. O. A. Youbi, X. Sun, *ACS Appl. Mater. Interfaces* **2014**, *6*, 1011.
- [74] Y. Zheng, Y. Jiao, L. Hua, T. Xing, Y. Chen, M. Jaroniec, S. Z. Qiao, *ACS Nano* **2014**, *8*, 5290.
- [75] R. Raccichini, A. Varzi, S. Passerini, B. Scrosati, *Nat. Mater.* **2015**, *14*, 271.
- [76] S. A. M. Silva, J. Perez, R. M. Torresia, C. A. Luengob, E. A. Ticianellia, *Electrochim. Acta* **1999**, *44*, 3565.
- [77] L. Sun, C. Wang, Y. Zhou, X. Zhang, J. Qiu, *J. Appl. Electrochem.* **2014**, *44*, 309.
- [78] W. Gajewski, P. Achatz, O. A. Williams, K. Haenen, E. Bustarret, M. Stutzmann, J. A. Garrido, *Phys. Rev. B* **2009**, *79*, 45206.

- [79] M. A. Angadi, T. Watanabe, A. Bodapati, X. C. Xiao, O. Auciello, J. A. Carlisle, J. A. Eastman, P. Keblinski, P. K. Schelling, S. R. Phillpot, *J. Appl. Phys.* **2006**, *99*, 114301.
- [80] O. A. Williams, *Diamond Relat. Mater.* **2011**, *20*, 621.
- [81] Z. Han, A. Fin, *Prog. Polym. Sci.* **2011**, *36*, 914.
- [82] C. Lu, C. Liu, *J. Chem. Technol. Biotechnol.* **2006**, *81*, 1932.
- [83] W. Wan, Y. Lin, A. Prakash, Y. Zhou, *J. Mater. Chem. A* **2016**, *4*, 18687.
- [84] Y. Wang, H. Liu, K. Wang, S. Song, P. Tsiakaras, *Appl. Catal., B* **2017**, *210*, 57.
- [85] D. D. L. Chung, *Appl. Therm. Eng.* **2001**, *21*, 1593.
- [86] M. Fujii, X. Zhang, H. Xie, H. Ago, K. Takahashi, T. Ikuta, H. Abe, T. Shimizu, *Phys. Rev. Lett.* **2005**, *95*, 065502.
- [87] G. Tao, L. Zhang, L. Chen, X. Cui, Z. Hua, M. Wang, J. Wang, Y. Chen, J. Shi, *Carbon* **2015**, *86*, 108.
- [88] B. You, F. Kang, P. Yin, Q. Zhang, *Carbon* **2016**, *103*, 9.
- [89] Y. Zhao, S. Huang, M. Xia, S. Rehman, S. Mu, Z. Kou, Z. Zhang, Z. Chen, F. Gao, Y. Hou, *Nano Energy* **2016**, *28*, 346.
- [90] J. C. Li, P. X. Hou, S. Y. Zhao, C. Liu, D. M. Tang, M. Cheng, F. Zhang, H. M. Cheng, *Energy Environ. Sci.* **2016**, *9*, 3079.
- [91] S. S. Shinde, C. H. Lee, A. Sami, D. H. Kim, S. U. Lee, J. H. Lee, *ACS Nano* **2017**, *11*, 347.
- [92] S. H. Lee, H. W. Kim, J. O. Hwang, W. J. Lee, J. Kwon, C. W. Bielawski, R. S. Ruoff, S. O. Kim, *Angew. Chem., Int. Ed.* **2010**, *49*, 10084.
- [93] Z. Chen, W. Ren, L. Gao, B. Liu, S. Pei, H. M. Cheng, *Nat. Mater.* **2011**, *10*, 424.
- [94] C. Xu, B. Xu, Y. Gu, Z. Xiong, J. Sun, X. S. Zhao, *Energy Environ. Sci.* **2013**, *6*, 1388.
- [95] B. G. Choi, M. Yang, W. H. Hong, J. W. Choi, Y. S. Huh, *ACS Nano* **2012**, *6*, 4020.
- [96] L. Tian, M. J. Meziani, F. Lu, C. Y. Kong, L. Cao, T. J. Thorne, Y. Sun, *ACS Appl. Mater. Interfaces* **2010**, *2*, 3217.
- [97] Y. Liu, Q. Feng, X. Xie, X. Ye, *Carbon* **2011**, *49*, 3371.
- [98] Y. Pan, H. Bao, L. Li, *ACS Appl. Mater. Interfaces* **2011**, *3*, 4819.
- [99] M. Kotal, A. K. Bhowmick, *J. Phys. Chem. C* **2013**, *117*, 25865.
- [100] V. C. Tung, L. Chen, M. J. Allen, J. K. Wassei, K. Nelson, R. B. Kaner, Y. Yang, *Nano Lett.* **2009**, *9*, 1949.
- [101] C. Zhang, S. Huang, W. W. Tjiu, W. Fan, T. X. Liu, *J. Mater. Chem.* **2012**, *22*, 2427.
- [102] M. K. Shin, B. Lee, S. H. Kim, J. A. Lee, G. M. Spinks, S. Gambhir, G. G. Wallace, M. E. Kozlov, R. H. Baughman, S. J. Kim, *Nat. Commun.* **2012**, *3*, 650.
- [103] I. Shakir, *Electrochim. Acta* **2014**, *129*, 396.
- [104] J. Wang, J. Tang, B. Ding, V. Malgras, Z. Chang, X. Hao, Y. Wang, H. Dou, X. Zhang, Y. Yamauchi, *Nat. Commun.* **2017**, *8*, 15717.
- [105] S. C. Wang, J. Yang, X. Y. Zhou, J. Li, *Int. J. Electrochem. Sci.* **2013**, *8*, 9692.
- [106] T. Hong, D. W. Lee, H. J. Choi, H. S. Shin, B. Kim, *ACS Nano* **2010**, *4*, 3861.
- [107] E. Nagelli, L. Huang, A. Dai, F. Du, L. Dai, *Part. Part. Syst. Character.* **2017**, *34*, 1700131.
- [108] D. A. Dikin, S. Stankovich, E. J. Zimney, R. D. Piner, G. Dommett, G. Evmenenko, S. T. Nguyen, R. S. Ruoff, *Nature* **2007**, *448*, 457.
- [109] J. Huang, Z. Xu, S. Abouali, M. A. Garakani, J. Kim, *Carbon* **2016**, *99*, 624.
- [110] X. Chen, M. Qiu, H. Ding, K. Fu, Y. Fan, *Nanoscale* **2016**, *8*, 5696.
- [111] Z. Yang, Y. Zhao, Q. Xiao, Y. Zhang, L. Jing, Y. Yan, K. Sun, *ACS Appl. Mater. Interfaces* **2014**, *6*, 8497.
- [112] D. D. Nguyen, N. H. Tai, S. Y. Chen, Y. L. Chueh, *Nanoscale* **2012**, *4*, 632.
- [113] K. Kumar, Y. Kim, X. Li, J. Ding, F. T. Fisher, E. Yang, *Chem. Mater.* **2013**, *25*, 3874.
- [114] D. H. Lee, J. E. Kim, T. H. Han, J. W. Hwang, S. Jeon, S. Choi, S. H. Hong, W. J. Lee, R. S. Ruoff, S. O. Kim, *Adv. Mater.* **2010**, *22*, 1247.
- [115] Z. J. Fan, J. Yan, L. J. Zhi, Q. Zhang, T. Wei, J. Feng, M. L. Zhang, W. Z. Qian, F. Wei, *Adv. Mater.* **2010**, *22*, 3723.
- [116] B. S. Mao, Z. Wen, Z. Bo, J. Chang, X. Huang, J. Chen, *ACS Appl. Mater. Interfaces* **2014**, *6*, 9881.
- [117] X. C. Dong, Y. W. Ma, G. Y. Zhu, Y. X. Huang, J. Wang, M. B. Chan-Park, L. H. Wang, W. Huang, P. Chen, *J. Mater. Chem.* **2012**, *22*, 17044.
- [118] W. Zhang, H. Xie, R. Zhang, M. Jian, C. Wang, Q. Zheng, F. Wei, Y. Zhang, *Carbon* **2015**, *86*, 358.
- [119] J. Jiang, Y. Li, C. Gao, N. D. Kim, X. Fan, G. Wang, Z. Peng, R. H. Hauge, J. M. Tour, *ACS Appl. Mater. Interfaces* **2016**, *8*, 7356.
- [120] Y. Zhao, C. Hu, L. Song, L. Wang, G. Shi, L. Dai, L. Qu, *Energy Environ. Sci.* **2014**, *7*, 1913.
- [121] C. Tang, Q. Zhang, M. Zhao, J. Huang, X. Cheng, G. Tian, H. Peng, F. Wei, *Adv. Mater.* **2014**, *26*, 6100.
- [122] M. Q. Zhao, X. F. Liu, Q. Zhang, G. L. Tian, J. Q. Huang, W. C. Zhu, F. Wei, *ACS Nano* **2012**, *6*, 10759.
- [123] T. Chen, Q. Zhang, M. Zhao, J. Huang, C. Tang, F. Wei, *Carbon* **2015**, *95*, 292.
- [124] H. Peng, J. Huang, M. Zhao, Q. Zhang, X. Cheng, X. Liu, W. Qian, F. Wei, *Adv. Funct. Mater.* **2014**, *24*, 2772.
- [125] C. Tang, Q. Zhang, M. Q. Zhao, G. L. Tian, F. Wei, *Nano Energy* **2014**, *7*, 161.
- [126] F. Du, D. Yu, L. Dai, S. Ganguli, V. Varshney, A. K. Roy, *Chem. Mater.* **2011**, *23*, 4810.
- [127] Y. Xue, D. Yu, L. Dai, R. Wang, D. Li, A. Roy, F. Lu, H. Chen, Y. Liu, J. Qu, *Phys. Chem. Chem. Phys.* **2013**, *15*, 12220.
- [128] Z. Yang, M. Liu, C. Zhang, W. Tjiu, T. Liu, H. Peng, *Angew. Chem., Int. Ed.* **2013**, *52*, 3996.
- [129] M. K. Liu, Y. E. Miao, C. Zhang, W. W. Tjiu, Z. B. Yang, H. S. Peng, T. X. Liu, *Nanoscale* **2015**, *7*, 1037.
- [130] L. Borchardt, Q. L. Zhu, M. E. Casco, R. Berger, X. Zhuang, S. Kaskel, X. Feng, Q. Xu, *Mater. Today* **2017**, *20*, 592.
- [131] S. Lawes, A. Riese, Q. Sun, N. Cheng, X. Sun, *Carbon* **2015**, *92*, 150.
- [132] M. Wei, F. Zhang, W. Wang, P. Alexandridis, C. Zhou, G. Wu, *J. Power Sources* **2017**, *354*, 134.
- [133] Y. Yang, X. Li, X. Zheng, Z. Chen, Q. Zhou, Y. Chen, *Adv. Mater.* **2018**, *30*, 1704912.
- [134] S. D. Lacey, D. J. Kirsch, Y. Li, J. T. Morgenstern, B. C. Zarket, Y. Yao, J. Dai, L. Q. Garcia, B. Liu, T. Gao, S. Xu, S. R. Raghavan, J. W. Connell, Y. Lin, L. Hu, *Adv. Mater.* **2018**, *30*, 1705651.
- [135] C. Zhu, T. Liu, F. Qian, T. Y. J. Han, E. B. Duoss, J. D. Kuntz, C. M. Spadaccini, M. A. Worsley, Y. Li, *Nano Lett.* **2016**, *16*, 3448.
- [136] C. Zhu, T. Y. J. Han, E. B. Duoss, A. M. Golobic, J. D. Kuntz, C. M. Spadaccini, M. A. Worsley, *Nat. Commun.* **2015**, *6*, 6962.
- [137] K. Chi, Z. Zhang, J. Xi, Y. Huang, F. Xiao, S. Wang, Y. Liu, *ACS Appl. Mater. Interfaces* **2014**, *6*, 16312.
- [138] Y. Zhang, L. Guo, S. Wei, Y. He, H. Xia, Q. Chen, H. B. Sun, F. S. Xiao, *Nano Today* **2010**, *5*, 15.
- [139] W. Gao, N. Singh, L. Song, Z. Liu, A. L. M. Reddy, L. Ci, R. Vajtai, Q. Zhang, B. Wei, P. M. Ajayan, *Nat. Nanotechnol.* **2011**, *6*, 496.
- [140] J. Lin, Z. Peng, Y. Liu, F. R. Zepeda, R. Ye, E. L. G. Samuel, M. J. Yacaman, B. I. Jakobson, J. M. Tour, *Nat. Commun.* **2014**, *5*, 5714.
- [141] R. Ye, D. James, J. M. Tour, *Acc. Chem. Res.* **2018**, *51*, 1609.
- [142] M. Andersson, S. B. Beale, M. Espinoza, Z. Wu, W. Lehnert, *Appl. Energy* **2016**, *180*, 757.
- [143] E. Yeager, *J. Mol. Catal.* **1986**, *38*, 5.
- [144] A. J. Bard, L. R. Faulkner, *Electrochemical Methods: Fundamentals and Applications*, Wiley, New York **2001**.
- [145] L. Qu, Y. Liu, J. B. Baek, L. Dai, *ACS Nano* **2010**, *4*, 1321.
- [146] J. S. Lee, K. Jo, T. Lee, T. Yun, J. Cho, B. S. Kim, *J. Mater. Chem. A* **2013**, *1*, 9603.
- [147] Y. Yang, H. Chang, *J. Mater. Res.* **2018**, *33*, 1247.



- [148] H. Li, W. Kang, L. Wang, Q. Yue, S. Xu, H. Wang, J. Liu, *Carbon* **2013**, 54, 249.
- [149] X. Zhou, Z. Bai, M. Wu, J. Qiao, Z. Chen, *J. Mater. Chem. A* **2015**, 3, 3343.
- [150] S. A. Wohlgemuth, T. P. Fellingner, P. Jaker, M. Antonietti, *J. Mater. Chem. A* **2013**, 1, 4002.
- [151] Q. Guo, D. Zhao, S. Liu, S. Chen, M. Hanif, H. Hou, *Electrochim. Acta* **2014**, 138, 318.
- [152] J. Liu, B. V. Cunnning, T. Daio, A. Mufundirwa, K. Sasaki, S. M. Lythf, *Electrochim. Acta* **2016**, 220, 554.
- [153] H. Jin, J. Li, F. Chen, L. Gao, H. Zhang, D. Liu, Q. Liu, *Electrochim. Acta* **2016**, 222, 438.
- [154] X. Zhou, S. Tang, Y. Yin, S. Sun, J. Qiao, *Appl. Energy* **2016**, 175, 459.
- [155] S. Tang, X. Zhou, N. Xu, Z. Bai, J. Qiao, J. Zhang, *Appl. Energy* **2016**, 175, 405.
- [156] W. Hu, N. Yoshida, Y. Hirota, S. Tanaka, N. Nishiyama, *Electrochem. Commun.* **2017**, 75, 9.
- [157] H. W. Liang, Z. Y. Wu, L. F. Chen, C. Li, S. H. Yun, *Nano Energy* **2015**, 11, 366.
- [158] L. T. Song, Z. Y. Wu, H. W. Liang, F. Zhou, Z. Y. Yu, L. Xu, Z. Pan, S. H. Yun, *Nano Energy* **2016**, 19, 117.
- [159] C. Hu, Y. Xiao, Y. Zhao, N. Chen, Z. Zhang, M. Cao, L. Qu, *Nanoscale* **2013**, 5, 2726.
- [160] D. Yu, L. Wei, W. Jiang, H. Wang, B. Sun, Q. Zhang, K. Goh, R. Si, Y. Chen, *Nanoscale* **2013**, 5, 3457.
- [161] H. W. Liang, X. Zhuang, S. Bruller, X. Feng, K. Mullen, *Nat. Commun.* **2014**, 5, 4973.
- [162] C. Xuan, Z. Wu, W. Lei, J. Wang, J. Guo, D. Wang, *ChemCatChem* **2017**, 9, 809.
- [163] M. Wu, K. Wang, M. Yi, Y. Tong, Y. Wang, S. Song, *ACS Catal.* **2017**, 7, 6082.
- [164] D. Eisenberg, W. Stroek, N. J. Geels, S. Tanase, M. Ferbinteanu, S. J. Teat, P. Mettraux, N. Yan, G. Rothenberg, *Phys. Chem. Chem. Phys.* **2016**, 18, 20778.
- [165] L. Li, P. Dai, X. Gu, Y. Wang, L. Yan, X. Zhao, *J. Mater. Chem. A* **2017**, 5, 789.
- [166] Y. Fu, C. Tian, F. Liu, L. Wang, H. Yan, B. Yang, *Nano Res.* **2016**, 9, 3364.
- [167] Z. Wen, S. Ci, Y. Hou, J. Chen, *Angew. Chem.* **2014**, 126, 6614.
- [168] D. Yu, L. Zhou, J. Tang, J. Li, J. Hu, C. Peng, H. Liu, *Ind. Eng. Chem. Res.* **2017**, 56, 8880.
- [169] X. Wu, S. Li, B. Wang, J. Liu, M. Yu, *Microporous Mesoporous Mater.* **2017**, 240, 216.
- [170] J. Liang, Y. Zheng, J. Chen, J. Liu, D. H. Jurcakova, M. Jaroniec, S. Z. Qiao, *Angew. Chem.* **2012**, 124, 3958.
- [171] X. Fu, X. Hu, Z. Yan, K. Lei, F. Li, F. Cheng, J. Chen, *Chem. Commun.* **2016**, 52, 1725.
- [172] M. Seredych, K. László, E. R. Castellón, T. J. Bandoz, *J. Energy Chem.* **2016**, 25, 236.
- [173] L. Chen, X. Cui, Y. Wang, M. Wang, R. Qiu, Z. Shu, L. Zhang, Z. Hua, F. Cui, C. Wei, J. Shi, *Dalton Trans.* **2014**, 43, 3420.
- [174] M. Seredych, K. Laszlo, T. J. Bandoz, *ChemCatChem* **2015**, 7, 2924.
- [175] I. Y. Jeon, S. Zhang, L. Zhang, H.-J. Choi, J.-M. Seo, Z. Xia, L. Dai, J.-B. Baek, *Adv. Mater.* **2013**, 25, 6138.
- [176] Y. Su, Y. Zhang, X. Zhuang, S. Li, D. Wu, F. Zhang, X. Feng, *Carbon* **2013**, 62, 296.
- [177] S. Jiang, Y. Sun, H. Dai, J. Hu, P. Ni, Y. Wang, Z. Lia, *Electrochim. Acta* **2015**, 174, 826.
- [178] H. Wu, L. Shi, J. Lei, D. Liu, D. Qu, Z. Xie, X. Du, P. Yang, X. Hu, J. Li, H. Tang, *J. Power Sources* **2016**, 323, 90.
- [179] S. Gao, H. Liu, K. Geng, X. Wei, *Nano Energy* **2015**, 12, 785.
- [180] Z. Wu, R. Liu, J. Wang, J. Zhu, W. Xiao, C. Xuan, W. Lei, D. Wang, *Nanoscale* **2016**, 8, 19086.
- [181] S. Wang, E. Iyyamperumal, A. Roy, Y. Xue, D. Yu, L. Dai, *Angew. Chem., Int. Ed.* **2011**, 50, 11756.
- [182] S. A. Wohlgemuth, R. J. White, M. G. Willinger, M. M. Titirici, M. Antonietti, *Green Chem.* **2012**, 14, 1515.
- [183] M. Wu, J. Qiao, K. Li, X. Zhou, Y. Liu, J. Zhang, *Green Chem.* **2016**, 18, 2699.
- [184] Z. Huang, H. Zhou, W. Yang, C. Fu, L. Chen, Y. Kuang, *ChemCatChem* **2017**, 9, 987.
- [185] M. Sahoo, S. Ramaprabhu, *Energy* **2017**, 119, 1075.
- [186] S. Fu, C. Zhu, J. Song, M. H. Engelhard, X. Li, P. Zhang, H. Xia, D. Du, Y. Lin, *Nano Res.* **2017**, 10, 1888.
- [187] Z. Wang, X. Cao, J. Ping, Y. Wang, T. Lin, X. Huang, Q. Ma, F. Wang, C. He, H. Zhang, *Nanoscale* **2015**, 7, 9394.
- [188] C. Xu, Y. Su, D. Liu, X. He, *Phys. Chem. Chem. Phys.* **2015**, 17, 25440.
- [189] I. M. Patil, M. Lokanathan, B. Kakade, *J. Mater. Chem. A* **2016**, 4, 4506.
- [190] H. Jiang, Y. Zhu, Q. Feng, Y. Su, X. Yang, C. Li, *Chem. – Eur. J.* **2014**, 20, 3106.
- [191] J. Wang, Z. X. Wu, L. L. Han, Y. Y. Liu, J. P. Guo, H. L. Xin, D. L. Wang, *Chin. Chem. Lett.* **2016**, 27, 597.
- [192] H. Jiang, Y. Wang, J. Hao, Y. Liu, W. Li, J. Li, *Carbon* **2017**, 122, 64.
- [193] Y. Qiu, L. Xin, F. Jia, J. Xie, W. Li, *Langmuir* **2016**, 32, 12569.
- [194] S. Fu, C. Zhu, J. Song, M. H. Engelhard, B. Xiao, D. Du, Y. Lin, *Chem. – Eur. J.* **2017**, 23, 10460.
- [195] Y. Jiang, L. Yang, T. Sun, J. Zhao, Z. Lyu, O. Zhuo, X. Wang, Q. Wu, J. Ma, Z. Hu, *ACS Catal.* **2015**, 5, 6707.
- [196] H. Zhao, C. Sun, Z. Jin, D. W. Wang, X. Yan, Z. Chen, G. Zhu, X. Yao, *J. Mater. Chem. A* **2015**, 3, 11736.
- [197] D. Yan, Y. Li, J. Huo, R. Chen, L. Dai, S. Wang, *Adv. Mater.* **2017**, 29, 1606459.
- [198] C. Tang, H. F. Wang, Q. Zhang, *Acc. Chem. Res.* **2018**, 51, 881.
- [199] B. Q. Li, C. Tang, H. F. Wang, X. L. Zhu, Q. Zhang, *Sci. Adv.* **2016**, 2, e1600495.
- [200] H. Jin, H. Huang, Y. He, X. Feng, S. Wang, L. Dai, J. Wang, *J. Am. Chem. Soc.* **2015**, 137, 7588.
- [201] E. Antolini, *Renewable Sustainable Energy Rev.* **2016**, 58, 34.
- [202] R. Liu, H. Zhang, S. Liu, X. Zhang, T. Wu, X. Ge, Y. Zang, H. Zhao, G. Wang, *Phys. Chem. Chem. Phys.* **2016**, 18, 4095.
- [203] B. Wang, S. Li, X. Wu, J. Liu, J. Chen, *J. Mater. Chem. A* **2016**, 4, 11789.
- [204] J. Zhang, H. Zhou, X. Liu, J. Zhang, T. Peng, J. Yang, Y. Huang, S. Mu, *J. Mater. Chem. A* **2016**, 4, 15870.
- [205] H. Ba, Y. Liu, L. T. Phuoc, C. D. Viet, J. M. Nhut, D. L. Nguyen, O. Ersen, G. Tuci, G. Giambastiani, C. P. Huu, *ACS Catal.* **2016**, 6, 1408.
- [206] Y. Yang, T. Liu, Q. Liao, D. Ye, X. Zhu, J. Li, P. Zhang, Y. Peng, S. Chen, Y. Li, *J. Mater. Chem. A* **2016**, 4, 15913.
- [207] M. Gong, H. Dai, *Nano Res.* **2015**, 8, 23.
- [208] M. Busch, N. B. Halck, U. I. Kramm, S. Siahrostami, P. Krttil, J. Rossmeisl, *Nano Energy* **2016**, 29, 126.
- [209] M. Tahir, L. Pan, F. Idrees, X. Zhang, L. Wang, J. J. Zou, Z. L. Wang, *Nano Energy* **2017**, 37, 136.
- [210] M. Gong, Y. Li, H. Wang, Y. Liang, J. Z. Wu, J. Zhou, J. Wang, T. Regier, F. Wei, H. Dai, *J. Am. Chem. Soc.* **2013**, 135, 8452.
- [211] Z. Xia, *Nat. Energy* **2016**, 1, 16155.
- [212] Y. Zhao, R. Nakamura, K. Kamiya, S. Nakanishi, K. Hashimoto, *Nat. Commun.* **2013**, 4, 2390.
- [213] T. Y. Ma, S. Dai, M. Jaroniec, S. Z. Qiao, *Angew. Chem., Int. Ed.* **2014**, 53, 7281.
- [214] S. Chen, J. Duan, M. Jaroniec, S. Z. Qiao, *Adv. Mater.* **2014**, 26, 2925.
- [215] X. Yu, M. Zhang, J. Chen, Y. Li, G. Shi, *Adv. Energy Mater.* **2016**, 6, 1501492.
- [216] J. Zhao, Y. Liu, X. Quan, S. Chen, H. Zhao, H. Yu, *Electrochim. Acta* **2016**, 204, 169.

- [217] Y. P. Zhu, Y. Jing, A. Vasileff, T. Heine, S. Z. Qiao, *Adv. Energy Mater.* **2017**, *7*, 1602928.
- [218] T. Y. Ma, J. Ran, S. Dai, M. Jaroniec, S. Z. Qiao, *Angew. Chem., Int. Ed.* **2015**, *54*, 4646.
- [219] K. J. Lee, Y. J. Sa, H. Y. Jeong, C. W. Bielawski, S. H. Joo, H. R. Moon, *Chem. Commun.* **2015**, *51*, 6773.
- [220] Z. Liu, Z. Zhao, Y. Wang, S. Dou, D. Yan, D. Liu, Z. Xia, S. Wang, *Adv. Mater.* **2017**, *29*, 1606207.
- [221] H. W. Park, D. U. Lee, Y. Liu, J. Wu, L. F. Nazar, Z. Chen, *J. Electrochem. Soc.* **2013**, *160*, A2244.
- [222] X. Li, Y. Fang, S. Zhao, J. Wu, F. Li, M. Tian, X. Long, J. Jin, J. Ma, *J. Mater. Chem. A* **2016**, *4*, 13133.
- [223] L. N. Han, X. Wei, B. Zhang, X. H. Li, Q. C. Zhu, K. X. Wang, J. S. Chen, *RSC Adv.* **2016**, *6*, 56765.
- [224] S. Patra, R. Choudhary, E. Roy, R. Madhuri, P. K. Sharma, *Nano Energy* **2016**, *30*, 118.
- [225] X. Huang, Q. Wang, D. Jiang, Y. Huang, *Catal. Commun.* **2017**, *100*, 89.
- [226] Z. Pei, H. Li, Y. Huang, Q. Xue, Y. Huang, M. Zhu, Z. Wang, C. Zhi, *Energy Environ. Sci.* **2017**, *10*, 742.
- [227] L. Garcia, in *Compendium of Hydrogen Energy* (Eds: V. Subramani, A. Basile, T. N. Veziro), Woodhead Publishing Series in Energy, Woodhead Publishing, Sawston, Cambridge, UK **2015**, pp. 83–107.
- [228] R. Paul, R. G. Reifenger, T. S. Fisher, D. Y. Zemlyanov, *Chem. Mater.* **2015**, *27*, 5915.
- [229] W. Zhou, J. Jia, J. Lu, L. Yang, D. Hou, G. Li, S. Chen, *Nano Energy* **2016**, *28*, 29.
- [230] B. Conway, B. Tilak, *Electrochim. Acta* **2002**, *47*, 3571.
- [231] N. Mahmood, Y. Yao, J. W. Zhang, L. Pan, X. Zhang, J. J. Zou, *Adv. Sci.* **2018**, *5*, 1700464.
- [232] P. Sudhagar, N. Roy, R. Vedarajan, A. Devadoss, C. Terashima, K. Nakata, A. Fujishima, in *Photoelectrochemical Solar Fuel Production: From Basic Principles to Advanced Devices* (Eds: S. Giménez, J. Bisquert) Springer International Publishing, Cham, Switzerland **2016**, pp. 105–160.
- [233] Y. S. Jun, J. Park, S. U. Lee, A. Thomas, W. H. Hong, G. D. Stucky, *Angew. Chem., Int. Ed.* **2013**, *52*, 11083.
- [234] S. N. Talapaneni, J. Kim, S. H. Je, O. Buyukcakir, J. Oh, A. Coskun, *J. Mater. Chem. A* **2017**, *5*, 12080.
- [235] K. Xie, H. Wu, Y. Meng, K. Lu, Z. Wei, Z. Zhang, *J. Mater. Chem. A* **2015**, *3*, 78.
- [236] Y. Tiana, Y. Ye, X. Wang, S. Peng, Z. Wei, X. Zhang, W. Liu, *Appl. Catal., A* **2017**, *529*, 127.
- [237] Y. Zhao, F. Zhao, X. Wang, C. Xu, Z. Zhang, G. Shi, L. Qu, *Angew. Chem.* **2014**, *126*, 14154.
- [238] J. Duan, S. Chen, M. Jaroniec, S. Z. Qiao, *ACS Nano* **2015**, *9*, 931.
- [239] D. Yan, S. Dou, L. Tao, Z. Liu, Z. Liu, J. Huo, S. Wang, *J. Mater. Chem. A* **2016**, *4*, 13726.
- [240] S. S. Shinde, A. Sami, J. H. Lee, *ChemCatChem* **2015**, *7*, 3873.
- [241] J. Zhang, Z. Zhao, Z. Xia, L. Dai, *Nat. Nanotechnol.* **2015**, *10*, 444.
- [242] Q. Liu, Y. Wang, L. Dai, J. Yao, *Adv. Mater.* **2016**, *28*, 3000.
- [243] X. Yan, Y. Jia, T. Odedairo, X. Zhao, Z. Jin, Z. Zhu, X. Yao, *Chem. Commun.* **2016**, *52*, 8156.
- [244] Z. Peng, S. Yang, D. Jia, P. Da, P. He, A. M. Al-Enizi, G. Ding, X. Xie, G. Zheng, *J. Mater. Chem. A* **2016**, *4*, 12878.
- [245] J. Zhang, L. Dai, *ACS Catal.* **2015**, *5*, 7244.
- [246] J. Lai, S. Li, F. Wu, M. Saqib, R. Luque, G. Xu, *Energy Environ. Sci.* **2016**, *9*, 1210.
- [247] B. Kumar, M. Asadi, D. Pisasale, S. S. Ray, B. A. Rosen, R. Haasch, J. Abiade, A. L. Yarin, A. S. Khojin, *Nat. Commun.* **2013**, *4*, 2819.
- [248] P. P. Sharma, J. Wu, R. M. Yadav, M. Liu, C. J. Wright, C. S. Tiwary, B. I. Yakobson, J. Lou, P. M. Ajayan, X. D. Zhou, *Angew. Chem., Int. Ed.* **2015**, *54*, 13701.
- [249] N. Sreekanth, M. A. Nazrulla, T. V. Vineesh, K. Sailaja, K. L. Phani, *Chem. Commun.* **2015**, *51*, 16061.
- [250] S. Zhang, P. Kang, S. Ubnoske, M. K. Brennaman, N. Song, R. L. House, J. T. Glass, T. J. Meyer, *J. Am. Chem. Soc.* **2014**, *136*, 7845.
- [251] Y. Liu, S. Chen, X. Quan, H. Yu, *J. Am. Chem. Soc.* **2015**, *137*, 11631.
- [252] W. Li, M. Seredych, E. R. Castellun, T. J. Bandosz, *ChemSusChem* **2016**, *9*, 606.
- [253] S. J. Amirfakhri, D. Binny, J. L. Meunier, D. Berk, *J. Power Sources* **2014**, *257*, 356.
- [254] P. Wu, P. Du, H. Zhang, C. Cai, *Phys. Chem. Chem. Phys.* **2013**, *15*, 6920.
- [255] T. Zhang, C. Li, Y. Gu, X. Yan, B. Zheng, Y. Li, H. Liu, N. Lu, Z. Zhang, G. Feng, *Talanta* **2017**, *165*, 143.
- [256] V. Broje, A. A. Keller, *Environ. Sci. Technol.* **2006**, *40*, 7914.
- [257] M. A. Zahed, H. A. Aziz, M. H. Isa, L. Mohajeri, S. Mohajeri, *Bioresour. Technol.* **2010**, *101*, 9455.
- [258] S. Wan, H. C. Bi, L. T. Sun, *Nanotechnol. Rev.* **2016**, *5*, 3.
- [259] Z. Q. Lin, Z. P. Zeng, X. C. Gui, Z. K. Tang, M. Zou, A. Cao, *Adv. Energy Mater.* **2016**, *6*, 1600554.
- [260] H. Liu, H. Wang, X. Zhang, *Adv. Mater.* **2015**, *27*, 249.
- [261] X. Wang, X. Lu, B. Liu, D. Chen, Y. Tong, G. She, *Adv. Mater.* **2014**, *26*, 4763.
- [262] X. Wang, B. Liu, R. Liu, Q. Wang, X. Hou, D. Chen, R. Wang, G. Shen, *Angew. Chem., Int. Ed.* **2014**, *53*, 1849.
- [263] W. Li, X. Xu, C. Liu, M. C. Tekell, J. Ning, J. Guo, J. Zhang, D. Fan, *Adv. Funct. Mater.* **2017**, *27*, 1702738.
- [264] J. H. Montoya, L. C. Seitz, P. Chakhranont, A. Vojvodic, T. F. Jaramillo, J. K. Nørskov, *Nat. Mater.* **2017**, *16*, 70.
- [265] M. R. Lukatskaya, B. Dunn, Y. Gogotsi, *Nat. Commun.* **2016**, *7*, 12647.
- [266] F. Podjaski, J. Kröger, B. V. Lotsch, *Adv. Mater.* **2018**, *30*, 1705477.
- [267] D. Yu, K. Goh, H. Wang, L. Wei, W. Jiang, Q. Zhang, L. Dai, Y. Chen, *Nat. Nanotechnol.* **2014**, *9*, 555.
- [268] X. Wang, K. Jiang, G. Shen, *Mater. Today* **2015**, *18*, 265.
- [269] C. Hu, X. Chen, Q. Dai, M. Wang, L. Qu, L. Dai, *Nano Energy* **2017**, *41*, 367.
- [270] H. Sun, X. You, J. Deng, X. Chen, Z. Yang, P. Chen, X. Fang, H. Peng, *Angew. Chem., Int. Ed.* **2014**, *53*, 1.
- [271] Z. Zhang, X. Chen, P. Chen, G. Guan, L. Qiu, H. Lin, Z. Yang, W. Bai, Y. Luo, H. Peng, *Adv. Mater.* **2014**, *26*, 466.
- [272] R. Paul, A. Roy, L. Dai, in *Carbon-Based Metal-Free Catalysts: Design and Applications* (Ed: L. Dai), Wiley, New York **2018**, Ch. 7.
- [273] L. Yang, D. Cheng, H. Xu, X. Zeng, X. Wan, J. Shui, Z. Xiang, D. Cao, *Proc. Natl. Acad. Sci. USA* **2018**, *115*, 6626.
- [274] H. B. Yang, S. F. Hung, S. Liu, K. Yuan, S. Miao, L. Zhang, X. Huang, H. Y. Wang, W. Cai, R. Chen, J. Gao, X. Yang, W. Chen, Y. Huang, H. M. Chen, C. M. Li, T. Zhang, B. Liu, *Nat. Energy* **2018**, *3*, 140.
- [275] R. Ye, J. Dong, L. Wang, R. M. Cruz, Y. Li, P. F. An, M. J. Yacamán, B. I. Yakobson, D. Chen, J. M. Tour, *Carbon* **2018**, *132*, 623.
- [276] Q. Liu, X. Liu, L. Zheng, J. Shui, *Angew. Chem.* **2018**, *130*, 1218.